DETERMINING THE RATE OF LIGAND INDUCED CHARGE TRANSFER EFFECTS ON QUANTUM DOTS

by

Cale Christopher Hudson Bowman

A thesis submitted to the faculty of
The University of North Carolina at Charlotte
in partial fulfillment of the requirements
for the degree of Master of Science in
Chemistry

Charlotte

2015

Approved by:

_____
Dr. Marcus Jones

_____
Dr. Daniel Rabinovich

_____
Dr. Haitao Zhang

_____
Dr. Thomas A. Schmedake

ABSTRACT

CALE CHRISTOPHER HUDSON BOWMAN. Determining the rate of ligand induced charge transfer effects on quantum dots. (Under the direction of Dr. MARCUS JONES)

In this report, charge carrier dynamics and rate of electron transfer is investigated between two bis(thioether)silane (R_2Bts^{Me}) ligands and 2.65 nm CdSe core quantum dots (QDs). Isothermal titration calorimetry (ITC) data is used to determine binding constant and percentage of occupied sites for these systems. The data is then used in conjunction with steady-state photoluminescence (SSPL) and time-resolved photoluminescence (TRPL) data in order to determine charge transfer rates as a function of bound ligand and intrinsic charge transfer rates that are dependent upon the species of ligand bound to QD surface. Interesting results were found through this analysis, and further testing using other ligands and CdSe QDs of different sizes may provide a more complete picture of this type of analysis with ligand-QD systems. Further experimental techniques are also postulated.

DEDICATION

For Iris, you put up with me quite well.

For my family, always being there when I needed you.

For UNC Charlotte, providing me this opportunity to expand my horizon.

For the Universe, please continue to guide me.

ACKNOWLEDGEMENTS

Thank you to my parents for offering consistent support and for reassuring me that I could handle the workload that came with collecting data, writing this thesis, teaching others and eliminating perhaps the most significant organic chemistry deficiency that the chemistry master's program at UNC Charlotte has ever seen. Thank you Iris, for putting up with me through this journey and providing necessary counsel.

Thank you to Robin Burns and Caroline Kennedy. Your efforts in making sure that I did not royally mess up with submitting paperwork and dealing with the Graduate School at UNC Charlotte are very appreciated. At the same time I would also like to thank the Graduate School at UNC Charlotte for providing the opportunity to work for a Master's degree in Chemistry in the first place.

I must thank Dr. Jon Merkert, Dr. Jordan Poler and Dr. Markus Etzkorn. I thank Dr. Etzkorn for giving me fine recommendations on how to handle myself in the program. Dr. Etzkorn also gave me the proper amount of pressure that I needed in order to finally become proficient at organic chemistry. Though the times were rough, I came out of it a more complete chemist thanks to those efforts. I thank Dr. Poler for meeting with me to talk about the ITC at times. His input was much appreciated near the end of my data gathering. I thank Dr. Merkert for teaching and supervising my work in cyclic voltammetry. I would have been completely lost trying to collect electrochemistry data otherwise.

Thank you to Linda Spurrier for your help in ordering materials and giving me life advice during said ordering. I would like to thank Dr. Craig Ogle for allowing me to use some butyllithium reagent for the synthesis of my ligands. I also thank Ms. Monica

Rabinovich for being a great chemistry lab coordinator. Teaching general chemistry lab as your subordinate was a fun experience.

I would like to thank my other master's student colleagues. Their occasional light conversation actually took the stress away from the work environment, and I could not imagine a better group of people to work amongst. I give a further acknowledgment to Casey Oian for helping me during synthesis of my thioether ligand compounds. Also thanks to the Jones Research Group: Drew, Danielle, Jose, G, Andy, Mohammed, Alexandra, Kathleen and Dr. Jones.

Finally, I would like to thank my research committee for their help and input. Thank you to Dr. Marcus Jones for being my research adviser and helping me sort through research questions. Sometimes you provided even more questions to consider, every single one of them intriguing and thought-provoking. I would like to think our interactions have expanded my thought process and my insight. Thank you to Dr. Dan Rabinovich for your tremendous help in synthesizing the aforementioned ligands. Much of your time was devoted to teaching me complicated and air-sensitive synthetic techniques as well as key distillation strategies to yield an efficient and well-controlled fractional distillation technique. Your collaboration in this project is quite helpful and your devotion to teaching students quite obvious. I would also thank Dr. Haitao Zhang and Dr. Tom Schmedake for their involvement as research committee members.

All the help that I've listed here and more that I have surely forgotten to mention truly show how much care went into my experience here at UNC Charlotte. I certainly will never forget the time and sacrifices that went into my Master's degree. Thank you.

TABLE OF CONTENTS

LIST OF ABBREVIATIONS

CB	conduction band
CdSe	cadmium selenide
Et_2Bts^{Me}	$(CH_3CH_2)_2Si(CH_2SCH_3)_2$
HDA	hexadecylamine
HOMO	highest occupied molecular orbital
ITC	isothermal titration calorimetry
LED	light-emitting diode
LUMO	lowest unoccupied molecular orbital
Me_2Bts^{Me}	$(CH_3)_2Si(CH_2SCH_3)_2$
NMR	nuclear magnetic resonance
Ph_2Bts^{Me}	$(C_6H_5)_2Si(CH_2SCH_3)_2$
PL	photoluminescence
QD	quantum dot
SSPL	steady-state photoluminescence
TCSPC	time-correlated single photon counting
TMEDA	tetramethylethylenediamine
TOP	tri-octylphosphine
TOPO	tri-octylphosphine oxide
TRPL	time-resolved photoluminescence

CHAPTER 1: INTRODUCTION

1.1. Quantum Dots

Quantum dots (QDs) are nanometer sized semiconductor macromolecules that exhibit size tunable optical properties that differ from those of bulk material.[1] Originally referred to as quantum "clusters,"[2] a great deal of research has been done on these types of materials since their discovery in the late 1980's. The high interest associated with QDs stems from the fact that these crystallites boast broad absorption and narrow photoluminescence bands. These properties make QDs efficient at emitting specific wavelengths of light, while also absorbing broad ranges of energy. Therefore, QDs are ideal for light harvesting applications such as photovoltaics[3-10] and light emitting applications such as lasers,[11-14] light emitting diodes (LEDs)[15-18] and biosensing.[19,20] The most commonly researched materials are cadmium sulfide (CdS), cadmium selenide (CdSe) and lead sulfide (PbS). These specific materials have attracted the most research attention due to their absorption and photoluminescence spectra lying within the visible and near infrared electromagnetic range. There is a potential for QD devices that has not been fully realized yet due to incomplete understanding of surface interactions and charge carrier dynamics. The ability to specialize QDs for a desired purpose is quite possible, as their natural optical properties can be tuned by changing their size. Bulk material and singular molecules typically only absorb and fluoresce at specific wavelengths without the possibility of change. Through advancement of knowledge on surface interactions we

can further specialize a QD device for an intended purpose. This combined with increased knowledge on charge transfer could allow QD devices to indeed be one of the top technological advancements in the near future.

1.1.1. Quantum Dot Surface Interactions

Understanding QD surface interactions are key when attempting to properly model systems involving QDs. As QD size decreases, their surface area to volume ratio increases. Even larger QDs however still boast a high surface area to volume ratio. As this work uses CdSe QDs, it is relevant to point out that a CdSe QD with a 2.5 nm diameter has approximately 50% of its atoms on the surface.[1] Since this work describes 2.65 nm diameter CdSe QDs, this estimate is not far from the system tested. Charge transfer is perhaps the most important surface interaction, and an understanding of this phenomenon is indeed vital toward the evolution of QD devices. Photovoltaics and LEDs rely heavily on charge transfer into and out of the device to function well. In order to understand the basic theory of charge transfer, band structure must first be understood.

1.1.2. Band Structure

In any material, be it a molecule, a QD, or bulk material, there are multiple states of high energy and states of low energy. In a molecule, individual energy levels are present, where the difference between the highest occupied molecular orbital (HOMO) and the lowest unoccupied molecular orbital (LUMO) defines the minimum amount of energy required to excite an electron from a low energy state to a high energy state. Unlike single molecules, bulk materials contain so many closely packed states that two bands are created. The edges of these bands are similar to the HOMO and LUMO of a single molecule due to the fact that the difference in energy between the band edges

defines the minimum energy required to excite an electron from the valence band into the conduction band. QD band structure could be described as a hybrid between the previous two types of systems. A QD may contain bands, or many closely packed energy states, but these bands do not describe the entire array of valence or conductive energy states. QDs also contain individual, or quantized, energy states located near the "band" edges. They are considered quantized as they have a specific amount of energy that separates them into individually recognized or discrete states. Once again, the difference between the lowest quantized conductive state and the highest quantized valence state defines the amount of energy required to excite an electron into the conduction band. This difference is referred to as the QD band gap.

When an electron absorbs sufficient energy from a photon to move it across the band gap into the conduction band a positively charged hole is left behind in the valence band. This electron-hole pair, known as an exciton, is then free to move around in bulk semiconductor material until it finally recombines. It is important to note that an exciton refers to an electron and hole pair that is interacting with each other, while an electron that is not associated with the hole is still simply considered an electron. The natural separation that initially occurs between electron and hole is a material dependent value called the Bohr exciton radius, approximately 5.6 nm in bulk CdSe.[21,22] In order for a crystallite particle to be considered a QD, it must have a diameter smaller than the Bohr exciton radius. Since QDs have diameters smaller than their associated Bohr exciton radius, they experience a phenomenon known as quantum confinement. In a fashion similar to that of the particle in a box, quantum confinement describes how energy levels spread out when the space around the particle becomes limited. This spreading of energy

states is what results in a quantum dot having a series of discrete energy levels, similar to a molecule, though more closely spaced together like that of bulk material.

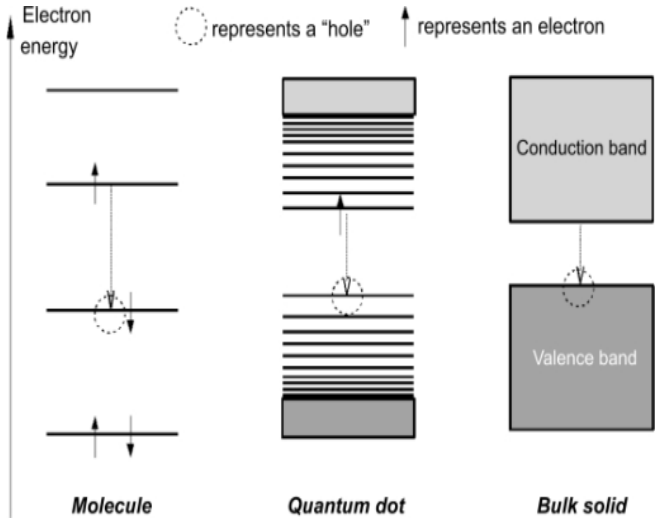

http://openi.nlm.nih.gov/detailedresult.php?img=2676646_ijn-1-451f1&req=4

Figure 1.1: From left to right, the energy levels of a molecule, the quantized states of a QD and the energy bands of bulk semiconductor material. In all instances, a single excitation of an electron is depicted followed by direct exciton recombination. This direct recombination would result in a photon being emitted from the sample at an energy equal to that of the band gap.

As mentioned earlier, QD optical properties are size tunable. This is due to energy differences associated with QD band gaps that arise when their size is changed. The following figure helps describe relative band gap energies dependent upon QD diameter.

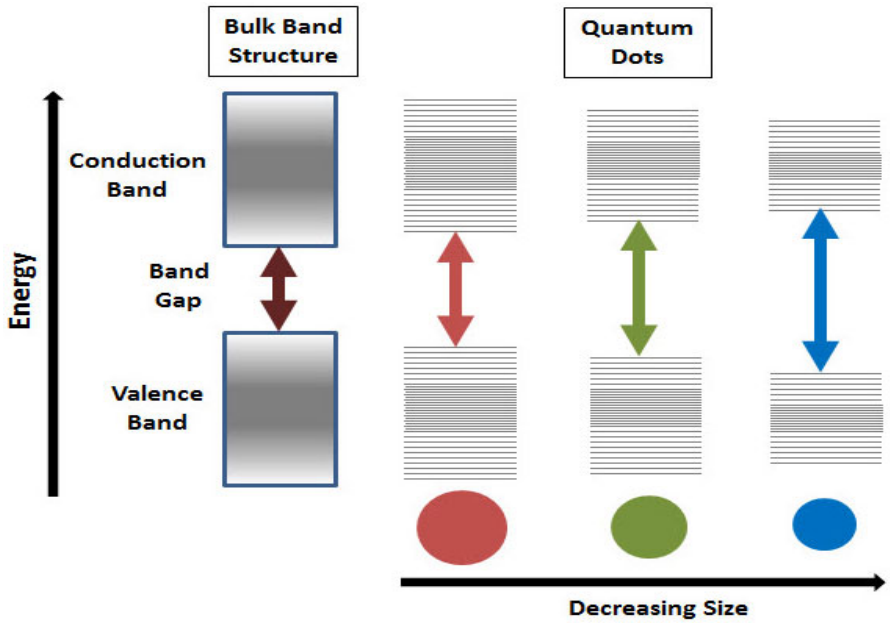

http://www.sigmaaldrich.com/materials-science/nanomaterials/quantum-dots.html

Figure 1.2: The band structure of bulk material is compared to band structures of QDs of the same material at decreasing sizes. As the QD diameter decreases, the band gap increases. Therefore, QDs of larger diameters have band structures that most closely resemble that of their corresponding bulk material.

1.1.3. Quantum Dot Photoluminescence

QD photoluminescence (PL) is a phenomenon that occurs when an electron directly recombines with a hole from the conduction band into the valence band after photo-excitation with sufficient energy for the electron to cross the band gap. When an electron recombines directly with its associated hole in this way a photon is emitted with energy equal to that of the band gap, a process referred to as radiative recombination. This is just one of the ways an electron may recombine, as nonradiative recombination is also possible. Experimental techniques such as absorbance, photoluminescence and time-resolved photoluminescence (TRPL) are able to probe these pathways. It has been determined that QDs may individually fluoresce, but if two or more QDs are bound together in a cluster, only the largest QD associated with the cluster is allowed to emit photons. The breaking of QD clusters is evident from blue shifts in emission wavelength,

as smaller QDs would then be able to fluoresce. The effect of size on emission wavelength is depicted in Figure 1.2.

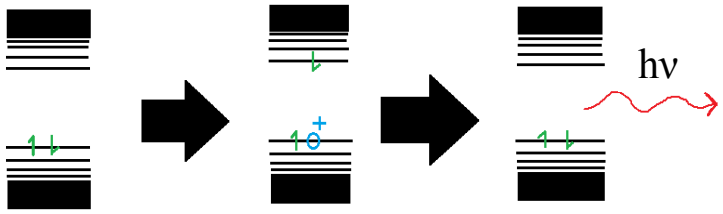

Figure 1.3: QD fluorescence is depicted in this series of band diagrams. An electron is photo-excited into the conduction band and relaxes directly back into the valence band releasing energy in the form of a photon.

1.1.4. Exciton Recombination Pathways

An exciton may recombine through a number of mechanisms. As previously described radiative recombination refers to a direct relaxation of an electron across the band gap. What may also occur is that an excited electron may enter a trap state from which nonradiative phonon coupling and Auger mechanisms allow exciton recombination without photon emission. These trap states may originate from impurities in the QD crystal lattice or from structural inconsistencies.

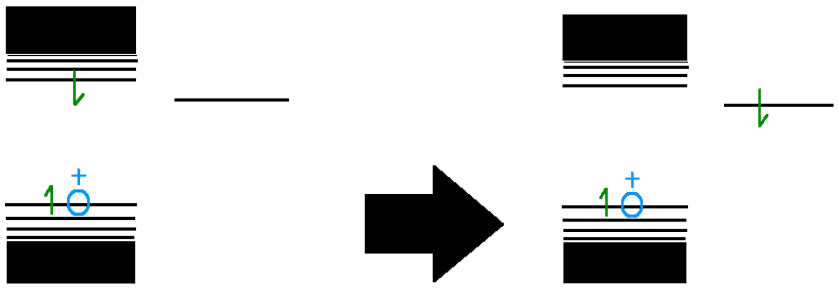

Figure 1.4: When a trap state exists within the band gap, charge separation may occur, leading to decreases in QD fluorescence and quantum yield.

1.2. Ligands

Vast majorities of QD species are synthesized using wet-chemical procedures.[18-22]

In all of these synthesis procedures there is an excess of many organic stabilizing ligands present in order to prevent material agglomeration and assist in QD crystallite formation. Typically trioctylphosphine oxide (TOPO),[23-25] hexadecylamine (HDA),[25,26] and trioctylphosphine (TOP)[23-25] are used in the synthesis of CdSe QDs. These QDs are then purified through precipitation with an immiscible solvent and centrifugation to remove unreacted precursors and other impurities.[23-28] Le Chatelier's principle predicts that when QDs are purified and diluted in pure solvent, QDs with fewer adsorbed, or bound, ligands will be favored in the system.[27,28] In order to maintain equilibrium, ligands will desorb from QD surface, which can result in unpassivated QDs that will tend to form aggregates.[29] This means that some form of passivation is desirable, as QD aggregation will affect exciton and also photoluminescence behavior since it has been shown that only the largest QD in an aggregate will fluoresce. Beyond passivation, it has been revealed that ligands are capable of affecting intraband relaxation rates[30-36] and charge carrier localization[37] as well as chemically controlling QD PL.[38] Techniques such as transient absorption and TRPL provide insight into charge carrier dynamics, but there is difficulty in trying to model these data as a function of QD ligand surface coverage. In order to model a function such as this, understanding QD exciton dynamics is critical, and would require a complete description of QD surface chemistry in order to properly study these spectroscopic measurements.

1.2.1. Passivating/Insulating Ligands

Passivation of a quantum dot refers to multiple ligands adsorbing to the surface of said QD. Passivation allows the QD to exist individually in a colloidal suspension while also eliminating surface trap states due to lattice defects or unbound surface sites. After

use in the synthesis of QDs, TOPO, HDA and TOP are commonly used for passivation purposes as they contain long carbon chains that make QDs stable in organic solvent. In addition to QD surface passivation, increased QD stability, and prevention of QD aggregation, ligands can have profound effects on QD optical properties. For example, the ligands previously mentioned, with the exception of TOPO, which will require further discussion, can be considered insulating ligands. TOPO, HDA and TOP have HOMO and LUMO energy levels that lie outside the range of QD band gaps. These HOMO and LUMO locations typically confine an exciton to the QD core,[7,9] increasing QD PL and quantum yield.

TOPO ligand presents an interesting case and is being discussed in detail due to recent work done by Williams et al.[39] It was determined that increasing TOPO concentration caused continuous lengthening of PL decays while also steadily reducing total PL intensity despite HOMO and LUMO levels lying beyond QD band edges. It was suggested that electron transfer into surface-localized TOPO-CdSe antibonding orbitals was responsible for this outcome. This seems plausible, as this effect would depend on the amount of adsorbed TOPO ligand and the nonexponential nature of the PL decays indicates this effect was not due to charge transfer into surface trap states. It is important to keep this phenomenon in mind, as similar studies focusing on HDA and TOP have not been conducted yet.

1.2.2. The Quenching Phenomenon and Quenching Ligands

In addition to the effects recently described some ligands are capable of separating electron and hole in the quantum dot. Such ligands are labeled as quenching ligands, and are known to decrease QD PL intensity and quantum yield. The two most

common types of quenching are static quenching and dynamic quenching. In the case of static quenching, a single ligand will separate an exciton so efficiently that once one ligand binds to the QD its PL vanishes completely. In this case the only variable that affects PL dependence as a function of quencher concentration is the association constant that describes a ligand's affinity for binding to the QD, as a single bound molecule provides such a fast nonradiative pathway that radiative recombination is unable to compete against it. Dynamic quenching is defined as a system where multiple ligands would be required to completely quench QD PL, as their rate of charge transfer is about the same as direct recombination. In such a case photoluminescence as a function of ligand concentration would depend on a quenching constant, as radiative recombination rate would be able to compete with the nonradiative rates induced by the ligands.

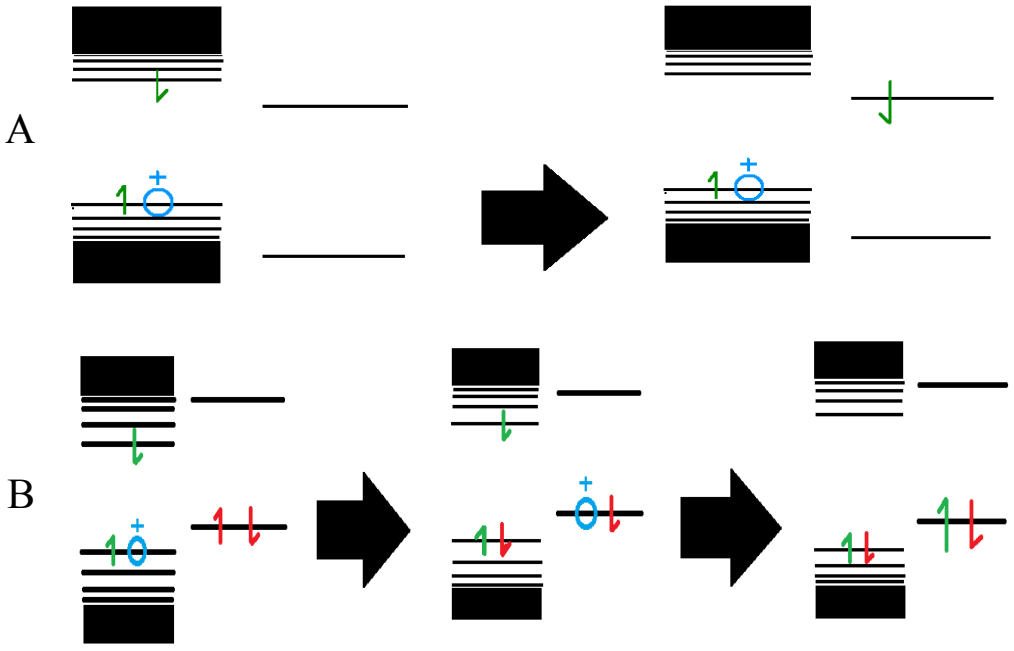

Figure 1.5: Band diagrams depicting a ligand with its LUMO existing within the QD band gap in (A) and a ligand with the HOMO lying within QD band gap. In either case quenching QD PL occurs.

Which subatomic particle is transferred out of the QD depends on the ligand's

HOMO and LUMO alignment relative to the band gap of the QD.[40-45] When the LUMO of the ligand lies within the QD band gap, an electron can transfer from the conduction band into the ligand. When the HOMO lies within the QD band gap, hole transfer to the ligand can occur. Electron transfer examples are viologen derivatives[27,40] and fullerenes,[46,47] while thiols[28,40,41,43,48-51] and amines[49,52-54] are prime examples of hole transfer ligands. If used correctly these ligands could contribute to charge injection or charge removal in QD devices, and usage in photovoltaic cells is of particular interest.

1.2.3. Understanding Local Ligand Environment

In order to accurately determine ligand contribution to QD PL dynamics, both an electronic environment and local ligand environment should be well understood. The electronic environment will be described using Marcus Theory, discussed later on. Characterizing the local ligand environment properly is also important, as probability of charge transfer into a ligand correlates positively to an increasing number of ligands bound to QD surface. The following figure helps describe how charge transfer rates are dependent upon number of ligands adsorbed.

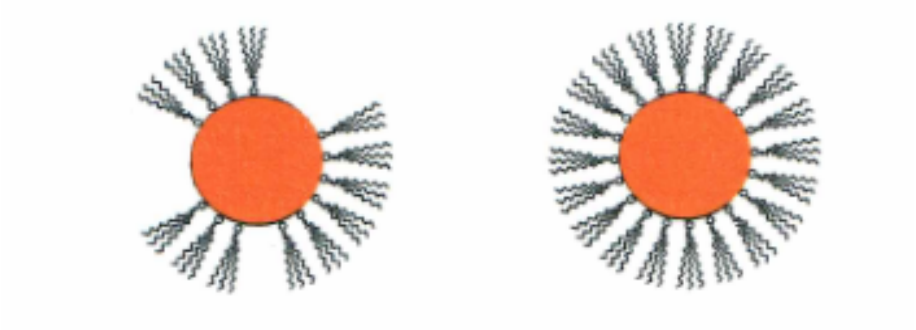

Figure 1.6: The QD on the left is only partially covered by ligand, while the QD on the right is fully saturated. As a result, charge transfer rates should be higher for the QD on the right than the system on the left.

1.2.4. Stern-Volmer Quenching Analysis

The Stern-Volmer kinetic relationships are well-known mathematical representations that apply to quantum yields of photophysical processes or photochemical reactions.[55] These processes vary with the concentration of a certain reagent that is either a substrate or quencher. In the simplest case, where a single ligand completely inhibits photoluminescence, $\frac{\phi^0}{\phi}$ or $\frac{I^0}{I}$ can be plotted vs. concentration of quencher, [Q] to yield a linear relationship:

$$\frac{\phi^0}{\phi} or \frac{I^0}{I} = 1 + K_{sv}[Q] \qquad \text{[eqn. 1-1]}$$

Where ϕ^0 and I^0 refer to the quantum yield and emission intensity of the system without any quencher added, respectively. These are two different variables, but are proportional. Variables ϕ and I are the same values with differing concentrations of quencher, [Q], present. The Stern-Volmer constant, K_{sv}, is the product of the true quenching constant k_q, and excited state lifetime, τ^0, in a system where dynamic quenching is evident. In this case, equation 1-1 can be replaced by the following expression:

$$\frac{\phi^0}{\phi} or \frac{I^0}{I} = 1 + k_q\tau^0[Q] \qquad \text{[eqn. 1-2]}$$

It is important to understand the origins of these equations and the type of chemical system they represent. In these cases the Stern-Volmer quenching model is linear with increasing concentration of quencher. This is due to their systems only allowing a single quenching ligand to attach to their base crystallite. QDs boast many different binding sites, which therefore yields the possibility to have multiple ligands attach to individual QDs. This main difference will be discussed later on, where the quenching model for this study is compared to the Stern-Volmer quenching expressions above.

1.3. Previous QD-Ligand Systems and Langmuir Analysis

In an attempt to improve the potential in QD devices, many studies have been conducted on various systems involving charge transfer. In similar fashion to this study, previous works have utilized absorbance, photoluminescence and time-resolved photoluminescence techniques to characterize PL quenching that occurs when charge transfer ligands bind to QDs.[27,28,40-45,56-59] Many of these works used basic Langmuir modeling to analyze the PL quenching data because this analysis can be used to obtain both the QD-ligand adsorption constant and charge transfer rates as a function of quenching ligand concentration.

Two prime examples of these studies are Koole et al.[43] and Koposov et al.[60] These groups used basic Langmuir analysis to study the interaction of hexanethiol and $Ru(bpy)_3$ derivatives with QDs, respectively. The addition of ligand to QDs caused PL intensity to drop, as shown (Figure 1.7(a)) in work by Koole et al. The PL data was then normalized (I_{norm}) and plotted vs. ligand concentration. The normalized data (Figure 1.7(b)) allows for the calculation of percent surface coverage, θ, according to equation 1-3 and shown in Figure 1.7(c).

$$\alpha\theta = \frac{1}{I_{norm}} - 1 \qquad \text{[eqn. 1-3]}$$

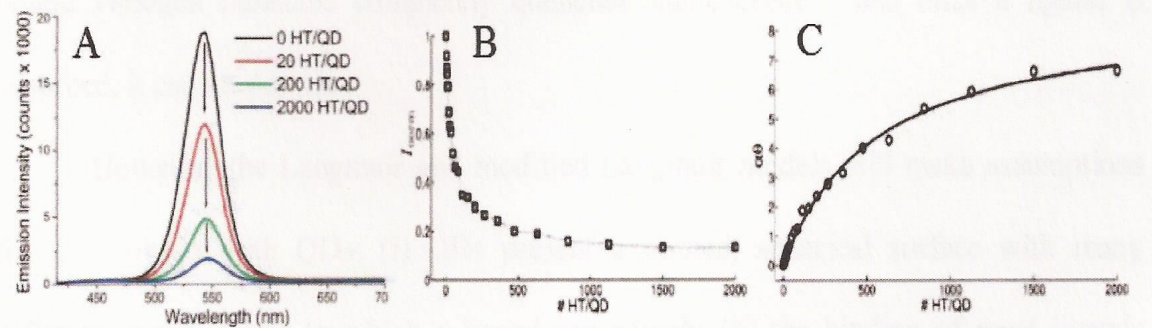

Figure 1.7: (a) shows diminishing PL intensity as hexanethiol was added to QDs. (b) depicts normalized data from (a) plotted as a function of ligand:QD ratio. (c) depicts the normalized PL data from (b) converted to a function of percent surface coverage using eqn. 1-3.

The effective Langmuir constant (K_L) was then calculated by fitting the data to equation 1-4, where C is ligand concentration and α is a fit constant. K_L can then be defined as the equilibrium-binding constant between the ligand of study and the QDs.

$$\alpha\theta = \alpha \frac{K_L C}{1+K_L C} \qquad \text{[eqn. 1-4]}$$

Basic Langmuir analysis is limited in its usefulness due to the assumptions that it makes to characterize charge transfer systems more easily. Langmuir analysis assumes that the surface where binding occurs is an infinitely long plane with a perfectly flat surface area. This assumption defines that the binding of a ligand does not change the number of binding sites available on the surface and that each surface site binds a ligand independent of the other binding sites. It was shown by Morris-Cohen et al.[27] that this assumption is unacceptable for QD systems. Results from their study revealed equilibrium constants calculated using a basic Langmuir model were dependent upon QD concentration. Morris-Cohen et al.[27] proposed a modification to the Langmuir model by using a binomial distribution and assuming two variables: the occurrence of static

quenching and that once a ligand is adsorbed, it cannot desorb. This allowed for equilibrium constants that were independent of QD concentration.

There are still many assumptions that exist between the basic Langmuir and modified Langmuir analyses that are invalid when describing QDs due to the following reasons: (i) QDs present spherical surfaces that are limited in area; (ii) QDs have many binding sites located on this limited surface, and as one site becomes occupied this most certainly has an effect on any further binding that would occur around the newly adsorbed ligand; (iii) static quenching is in most cases unreasonable, as the binding of one ligand cannot simply be assumed to completely quench all photoluminescence from the QD; (iv) by Le Chatelier's principle, a concept taught in introductory chemistry courses, it is known that systems actively strive for equilibrium between bound and unbound species, and it is not plausible to assume the permanent binding of ligands without the chance of desorption from the surface.

While these analyses provide reasonable thermodynamic binding parameters for systems involving quenching of QD PL, new obstacles arise when trying to provide these same parameters for ligands that do not quench QD PL. Ligands such as TOP and HDA are difficult to characterize with Langmuir analysis.

This study will not use Langmuir analysis and will instead use an independent binding site model[39,61] through the incorporation of isothermal titration calorimetry (ITC), a technique discussed in section 1.8. ITC provides a means of discerning thermodynamic information for all types of ligands; therefore, an independent binding site model may be a superior method for describing ligand-QD interaction compared to Langmuir analysis. Our research group has had a previous successful study using such a

method have also been done, where ITC was used to describe the thermodynamics of ligands adsorbing to QD surface.[39]

1.4. Marcus (Electron Transfer) Theory

Although this method was not used for data analysis associated with this project, a general understanding is important and hopefully future students may use this as a first introduction into electron transfer. Marcus theory can be used to determine charge transfer rates, Gibb's free energy and activation energy associated with systems.[62] In this electron transfer theory each energy state in the system is described by a parabola that represents every possible atomic arrangement of that state along with associated levels of energy. QD systems are typically modeled using parabolas to represent a ground state, an excited state, and a charge separated or trap state. Some important factors to consider when applying Marcus theory are the Gibb's free energy, reorganization energy, activation energy, and the electronic coupling matrix element. Gibb's free energy refers to the favorability of the charge transfer process, while activation energy defines the amount of energy required for charge transfer to occur. Reorganization energy is defined as the amount of energy necessary to force the excited state to have the same nuclear arrangement as the minimum energy level of the trap state. A qualitative representation of Marcus theory is shown below and plotted as a function of bath polarization. Bath polarization is defined as the change in atomic arrangement as charge shifts in the energy state.

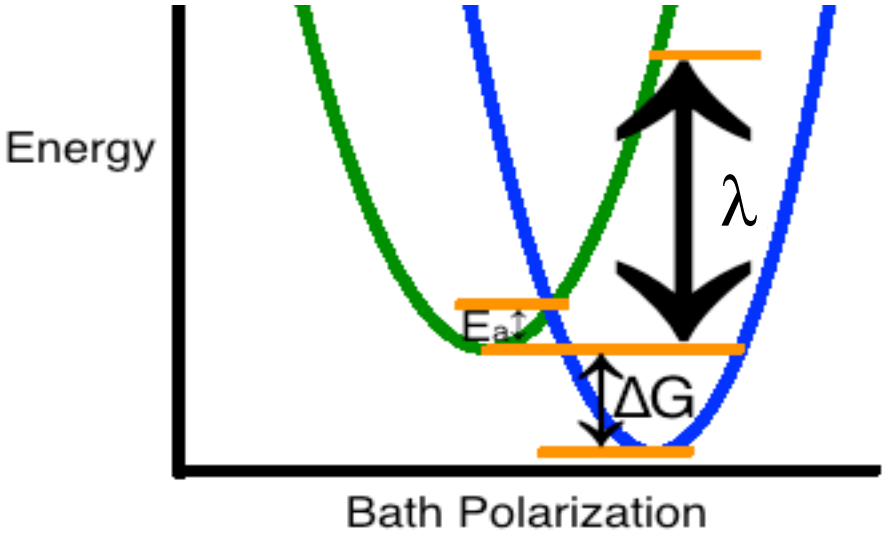

Figure 1.8: A brief qualitative diagram of Marcus theory describing the values that are important when using Marcus theory to describe charge transfer. Bath polarization describes the nuclear configuration caused by shifts in electronic environments. The parabolas represent every possible energy level and atomic arrangement of the state, with the excited state shown in green and the trap state shown in blue. The energy difference between the minima of the parabolas is the Gibb's free energy, ΔG. The energy difference between the minimum of the excited state and where the two parabolas intersect is the activation energy, E_a, or the energy required for charge transfer. The reorganization energy, λ, is defined as the amount of energy required to make the excited and trap states have the same atomic arrangement.

1.4.1. The Inverted Region of Marcus Theory

Gibb's free energy can be determined by calculating the energy difference between the minima of the excited state and trap state parabolas. Marcus theory predicts that as the charge transfer process becomes more favorable (increase in ΔG), the activation energy associated with the transfer decreases. When ΔG increases beyond the value of the reorganization energy, the activation energy associated with the charge transfer then increases as opposed to decreases. This is known as the Marcus inverted region.

Originally, the Marcus inverted region could not be confirmed experimentally as reactions were limited by electron diffusion before reaching the inverted region,

regardless of charge transfer favorability. Finally, in the mid-1980's, new systems were created where the donor and acceptor were separated by a bridging unit. These new systems confirmed the existence of the Marcus inverted region. Intermolecular charge transfer is limited by solvent diffusion while intramolecular charge transfer is not, allowing access to the inverted region.[62,63] The inverted region is highly accessible to QD systems as acceptor and donor are often attached to each other, similar to the bridged systems that initially supported the existence of the inverted region.

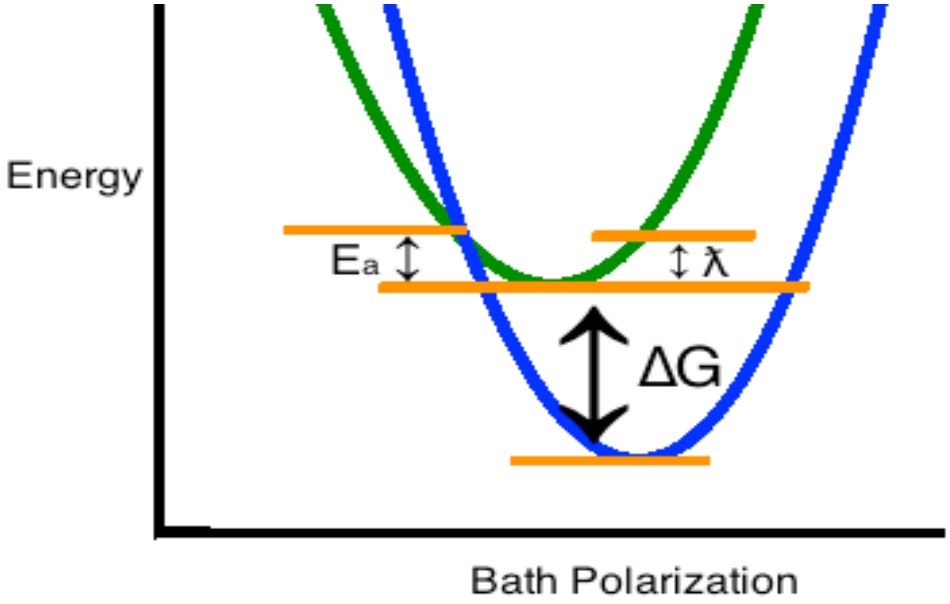

Figure 1.9: A qualitative example depicting the inverted region of Marcus theory. As favorability of the charge transfer process increases, the Gibb's free energy overcomes the reorganization energy. The activation energy of charge transfer then increases with increasing favorability rather than decreases.

1.5. Absorbance Spectroscopy

Absorbance spectroscopy is useful when used for QD systems as it can be used to determine QD diameter[56] and sample concentration through the use of Beer's Law.[56] Further applications can be to correct PL spectra for sample absorbance and check for absorbing anomalies in a sample. The technique measures the negative log of a sample's

transmittance at each wavelength of light spread over a set range of wavelengths. Transmittance is the ratio of the number of photons that pass through sample solution compared to the number of photons that pass through a "blank" containing only solvent.

1.6. Steady State Photoluminescence Spectroscopy

In this form of photoluminescence measurement, samples are excited by a single wavelength of light selected by an excitation monochromator located between the light source and sample. Photoluminescence of the sample is then detected perpendicular to the excitation source. Collecting perpendicular to the excitation allows for detected photons to be from QD photoluminescence rather than from transmitted light originating from the excitation source. Each emission wavelength of light is then measured individually by scanning the sample PL with an emission monochromator over a set range of wavelengths before the emitted light reaches the detector. These measurements are corrected for source lamp intensity by simultaneous recording of lamp intensity using a diode detector. After measurements are taken, PL spectra are corrected for detector sensitivity and sample absorbance.

1.7. Time-Resolved Photoluminescence

Time-resolved photoluminescence (TRPL) uses a pulsed light source to excite a sample. Photoluminescence is then measured perpendicular to the excitation, and plotted as a function of time. Each photon is counted in a technique known as Time Correlated Single Photon Counting (TCSPC). This technique records the amount of time that passes between the detector recording a photon and the excitation source releasing another pulse of light. Over time a histogram is built that profiles a sample's PL over time in the form of a decay. The information determined through this technique helps with understanding

charge carrier relaxation dynamics at work in the sample.

1.8. Isothermal Titration Calorimetry

Isothermal Titration Calorimetry (ITC) is a very precise and sensitive technique that measures enthalpy changes of reactions. Historically, this technique has been used by biochemists to determine binding parameters (equilibrium and binding constants) of protein-substrate interactions directly.[64] This technique is useful for the purposes of this study as ITC can be used to characterize the binding of any ligand that interacts with QDs, regardless of its affect on PL. Due to its primary use as a biochemical instrument, the vast majority of ITC studies have involved protein binding in aqueous systems. A few studies have been done with nanoparticles in aqueous conditions,[65,66] as well as a few studies with nanoparticles in organic solvent,[39,67-69] only two of which actually focusing on QDs.[39,69]

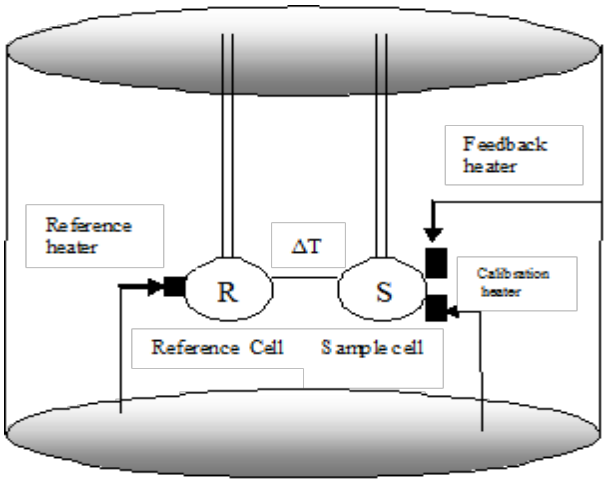

http://www.intechopen.com/books/thermodynamics-kinetics-of-dynamic-systems/calorimetric-investigations-of-non-viral-dna-transfection-systems

Figure 1.10: In ITC, two cells covered in gold are filled with sample solution. One of these cells is the sample cell, where titrant is added, while the other cell is named the reference cell. A "dummy" needle is inserted into the reference cell to account for heat exchange between solution and titration syringe. Heat differences that occur in the sample cell relative to the reference cell due to titrant injections are then corrected to create a plot of isothermic peaks representing the amount of heat required to keep the sample and reference cells at the same constant temperature as a function of time.

Though ITC is useful, an extraordinary amount of care and attention to detail is required to obtain accurate results. All commercially available ITC models utilize differential power compensation,[70] where the primary measurement is heat rate derived from the power supplied by a control heater that is used to maintain a constant temperature for a reaction system. For TA Instruments models, the power from the control heater is compensated by an actively controlled cooling mechanism. There are three key temperatures that are controlled while the instrument is running. A top plate is proportionally set to a temperature higher than the temperature set point of the reaction cell. The temperature of the cell block is set to the same temperature as the reaction cell. A bottom plate is then proportionally set to a temperature lower than the temperature of the cell block.

Theoretically, the cooling mechanism remains constant and changes that occur in the control power in order to maintain an isothermal condition would accurately measure heat from reactions. Real systems naturally differ from ideal conditions for two main reasons.[70] The first is that the control circuit cannot exactly compensate sudden changes in heat input from an injection. This will cause transient nonisothermal conditions capable of transferring heat between sample cell and surroundings, which can alter the cooling power. The second is that differences in heat distribution between the system and the control heater cause heat exchange with the surroundings and reference cell. This heat exchange will differ from the heat effects from a chemical reaction and the heat effects of the control heater. Proper calibration of an ITC can be easily determined through titrations of isopropanol into a sample cell filled with isopropanol. As long as integrated peak areas caused by exothermic diffusion remain below 5 μJ then the

instrument is typically ready for experimentation, though transfer into the solvent of your system will take time.

1.9. Systems of Interest

As previously stated, quenching ligands provide a means of charge transfer out of QDs, providing nonradiative exciton recombination pathways that are necessary for potential devices. Due to this, a study on the effects of a series of bis(thioether)silane (R_2Bts^{Me}) ligands on QD charge carrier dynamics was envisioned.[61] The ligands of interest, $(CH_3)_2Si(CH_2SCH_3)_2$ (Me_2Bts^{Me}), $(CH_3CH_2)_2Si(CH_2SCH_3)_2$ (Et_2Bts^{Me}), and $(C_6H_5)_2Si(CH_2SCH_3)_2$ (Ph_2Bts^{Me}) are unique in that the portion of the ligand that binds to the QD remains the same while the R group directly bound to the central silicon atom modifies the HOMO level of the lone pair located on the sulfur atoms relative to the QD band gap. It is clear theoretically and experimentally that the HOMO energy of the Et_2Bts^{Me} is greater than for Me_2Bts^{Me} due to a greater magnitude of electron donation. It was difficult to conceptually understand whether the HOMO level of the Ph_2Bts^{Me} compound would have the greatest energy of the three compounds or the lowest energy of the three compounds, due to the phenyl groups having both electron donating and withdrawing natures. Trends that will be discussed later in this report support the idea that the phenyl groups bound to the central silicon atom are indeed electron withdrawing.

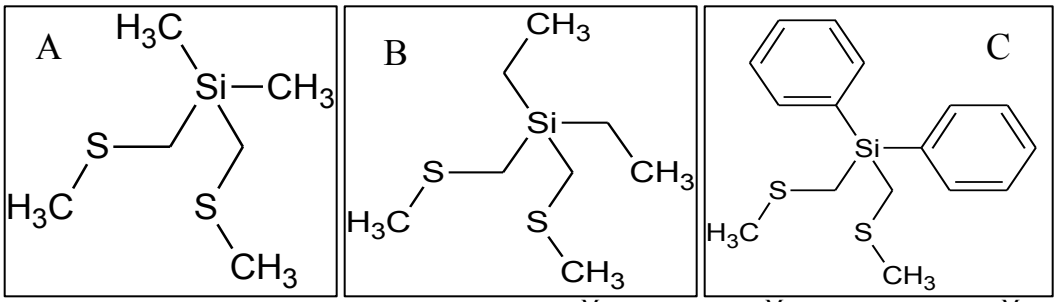

Figure 1.11: Molecular structures of (A) Me_2Bts^{Me-}, (B) Et_2Bts^{Me}, and (C) Ph_2Bts^{Me} ligands are shown.

Prior PL studies that involved the binding of Ph_2Bts^{Me} and Me_2Bts^{Me} to gold showed measured quantum yields far lower than expected, explained by ligand induced molecular recombination pathways. Complexes of these ligands with Cd(II), Pb(II), Hg(II), Cu(I) and Ag(I) have also been studied.[71,72] It is believed that these ligands provide electron transfer from the ligand into the valence band of the QD, leaving a hole in the bonding orbital formed between the 5s orbital of the Cd(II) and the sp^3 hybridized orbital of the sulfur. Nonradiative recombination between the previously photo-excited electron and the newly positioned hole can then occur.

For this study, the PL dynamics of a series of R_2Bts^{Me} bound to CdSe core QDs with a diameter of 2.7 nm was studied using absorbance, steady state photoluminescence, and TCSPC. These data were then used in conjunction with ITC measurements in order to give a thorough picture of surface conditions, added exciton recombination pathways, and intrinsic charge transfer rates that produced certain PL effects. It is expected that QD PL intensity will drop for each R_2Bts^{Me} ligand species,[61] however further information such as charge transfer rates, carrier dynamics, and site association (or binding) constants have yet to be properly explored.

CHAPTER 2: EXPERIMENTAL

2.1. General Instrumentation

Absorbance measurements were taken on a Cary 50 UV-Vis spectrometer. Photoluminescence and TCSPC data were taken on a Jobin-Yvon Fluorolog 3 with a Hamamatsu R928 PMT detector. Steady state PL measurements were taken using a xenon-arc lamp as the excitation source. The TCSPC measurements were taken using a pulsed light source (IBH). For ITC measurements, the Nano ITC-LV from TA Instruments was used, which is an ITC designed specifically for low volume work as opposed to a standard volume model. Proton NMR measurements were taken on a JEOL ECX 300 NMR spectrometer. Cyclic Voltammetry scans were done using a graphite electrode with tetrabutylammonium hexafluorophosphate ($TBAPF_6$) as the electrolyte in acetonitrile solvent at a scan rate of 200 mV/s with a ferrocene standard present.

2.2. Synthesis of R_2Bts^{Me}

The Me_2Bts^{Me}, Et_2Bts^{Me} and Ph_2Bts^{Me} ligands have been synthesized and characterized prior to this work.[61,71,72] The following procedure is a general synthesis for these ligands.

In a 500 mL round-bottom flask, under a constant flow of argon, a solution of $LiBu^n$ in hexanes (2.5M, 100 mL, 250 mmol) was added using a syringe to a stirred cold (0 °C) solution of Me_2S (25 mL, 340 mmol) and TMEDA (40 mL, 265 mmol) in pentane solvent (80 mL), resulting in the formation of a pale yellow solid suspended in a yellow,

cloudy solution. The suspension was allowed to warm to room temperature and then refluxed for 2 hours to complete the deprotonation reaction yielding the $LiCH_2SMe$ intermediate reagent. A cold (0 °C) solution of R_2SiCl_2 (R = Me, Et, or Ph, 125 mmol) in pentane solvent (80 mL) was then added in small portions via cannula to the above reaction mixture cooled to -60 °C in a Pr^iOH/dry ice bath, resulting in the gradual formation of a white precipitate (LiCl) and a yellow supernatant. The system was allowed to warm to room temperature and was then refluxed for 3 hours, after which it was allowed to cool back to room temperature. The light yellow supernatant was then separated by gravity filtration and the white residue was extracted into pentane (50 mL). The volatile components from the combined filtrate and extract were removed under reduced pressure to yield an orange liquid (high viscosity for the Ph_2Bts^{Me} synthesis), which was transferred to a 50 mL round-bottom flask. Fraction vacuum distillation of the oily liquid yielded the desired product as a pale yellow, spectroscopically pure liquid.

^1H NMR spectra were obtained for all three ligands in $CDCl_3$ solvent and were comparable to previous characterizations of each species.[61,71,72] The densities of Me_2Bts^{Me}, Et_2Bts^{Me} and Ph_2Bts^{Me} in their pure form were experimentally determined to be 1.00 g/mL, 0.97 g/mL, and 1.03 g/mL, respectively.

2.3. Quantum Dot Synthesis

CdSe core QDs were synthesized according to the procedure described in Clapp et al.[24] Briefly, a coordinating ligand mixture was prepared by mixing 10.00 g HDA, 12.00 g TOPO and 3.50 mL TOP. This mixture was heated to 120.0 °C and degassed for 30 minutes, then heated to 300.0 °C for injection under nitrogen. Meanwhile, in a second flask, 0.675 g $Cd(acac)_2$, 9.00 mL TOP, 1.200 g 1,2-hexanedecanediol and 5.00 mL Se

solution in TOP (1.0 M) were heated to 100.0 °C then cooled to 80 °C under vacuum. This mixture was quickly injected into the coordinating ligand mixture and nanocrystals were allowed to grow for 10 minutes at 250 °C. This resulted in 2.7 nm CdSe core QDs that were purified by addition of a nonsolvent followed by centrifugation. To limit photo-degradation and prolong their life the QD precipitate was stored in the dark. The QDs would then be dispersed in hexane for sample preparation.

2.4. QD Sample Preparation for Isothermal Titration Calorimetry

The presence of TOPO already passivating the QD surface and excess TOPO existing in the QD stock solution creates a competitive environment in regards to the ability for the R_2Bts^{Me} ligands to bind to the CdSe QDs. TOPO is used during the synthesis of the QDs and later used to stabilize QDs in organic solvent.[24] Rather than synthesizing QDs with different surface ligands a QD purification method utilizing acetone as the nonsolvent was used. The addition of acetone at a volume twice as much as the QD solution volume removed excess and weakly bound TOPO efficiently. Centrifugation of the sample is then done followed by decanting of supernatant to yield purified QD precipitate. The wash was repeated a second time in order to spectroscopically eliminate TOPO (and perhaps some residual TOP) from the system, confirmed by ^{31}P NMR. The purified QDs were then redispersed in hexane solvent and passivated with R_2Bts^{Me} ligand at a ligand:QD molar ratio of 3000:1. Theoretically, simply adding higher concentrations of the R_2Bts^{Me} ligand would be sufficient to counter the problem of a competitive environment brought about by TOPO, however the resulting system would be much more difficult to model.

Although removing TOPO causes the QDs to become unstable in organic

solution, it was observed that as the R_2Bts^{Me} ligand adsorbs to the QD surface, a colloidal suspension was achieved again in organic solvent. Further studies using ^{31}P NMR to quantify the concentration of TOPO present on unstable QDs along with photoluminescence and absorbance spectrometry to determine quantum yield measurements would provide more insight into the functionality of QDs and the ability of R_2Bts^{Me} ligand to stabilize QDs in organic solvents.

For ITC measurements 20 mL CdSe QD sample solutions were prepared in hexane solvent by adding the appropriate volume of R_2Bts^{Me} ligand to create a 3000:1 ligand:QD molar ratio (QD concentration varied for each solution, though was always in the range of $5x10^{-7}$ M to $8x10^{-7}$ M).

2.5. R_2Bts^{Me} Ligand Solution Preparation for Isothermal Titration Calorimetry

20 mL stock solutions of 5mM (0.005 M) Me_2Bts^{Me} and Et_2Bts^{Me} ligand were prepared in hexane solvent from pure ligand utilizing their experimentally determined densities. A conversion from 0.005 M to mmol/mL yields 0.005 mmol/mL, which was then multiplied by the final desired volume of 20 mL to equal 0.1 mmol. The 0.1 mmol were then converted to grams using the molar mass of each species. Using the experimentally determined densities, the volume of each ligand needed was determined. The volumes calculated represent the amount of ligand added to 20 mL of hexane to prepare the stock solutions.

2.6. Isothermal Titration Calorimetry Measurements

ITC measurements were made using an instrument designed specifically for low volume work. There are two 164 μL gold reaction cells held at a precisely controlled temperature located in the instrument, one for sample and one for reference. Both of

these cells were overfilled (200 μL) with QD solution that had QDs passivated at a 3000:1 R_2Bts^{Me} ligand:QD molar ratio. The ligand that was being studied was also the ligand initially added for passivation. The 5mM solution of the ligand of interest was then added via incremental titration into the sample cell using a specially designed 50 μL titration syringe with a built in stir tip. Each of these experiments was run using 25 injections, each set at 2 μL volume. All measurements were made at 20 °C operating temperature and with a 250-rpm stir rate. The instrument then measured the amount of power required to keep both the sample and reference cells at the same temperature over time. The time between each injection was set to 300 seconds to ensure the system returned to equilibrium, and therefore the baseline, before the next injection in the experiment. A "dummy" needle was inserted into the reference cell in order to account for any heat exchange that occurred between the QD sample solution and the needle of the syringe. Between each experimental run thorough rinsing of the syringe, sample cell, reference cell, and "dummy" needle was done using degassed hexane. This was done to remove excess ligand or QDs left over in the ITC system. Furthermore, control scans of 5mM R_2Bts^{Me} solution titrated into hexane solvent were also collected. The heats from the control scans were subtracted from the titration of R_2Bts^{Me} into QD solution in order to correct for heats caused by dilution or diffusion.

2.7. Sample Preparation for Photoluminescence Measurements

Multiple series of solutions consisting of 2 mL of 2.7 nm diameter QD solution (containing QDs in hexane at concentration of $5.5x10^{-7}$ M) and 1 mL of solution that was a combination of hexane solvent and ligand solution diluted in hexane. Studies using Me_2Bts^{Me} investigated ligand:QD molar ratios of 100:1 to 100,000:1 (using stock ligand

solution set at 0.110 M). Studies using Et_2Bts^{Me} investigated ligand:QD molar ratios of 50:1 through 50,000:1 (using stock ligand solution set at 0.055M). As the volume of ligand solution added to the 2 mL of QD solution increased, the volume of hexane solvent added to make up the 1 mL of hexane/ligand solution combination decreased. These series of solutions probed a range of 0 μL of ligand solution added to 1,000 μL of ligand solution added.

2.8. Steady State and Time-Resolved Photoluminescence Measurements

Photoluminescence measurements were collected using a Jobin-Yvon Fluorolog 3 with a Hamamatsu R928 PMT detector. An excitation wavelength of 425 nm from a xenon-arc lamp was used for steady state photoluminescence scans set to an emission range of 450 nm to 800 nm in 1 nm increments with 0.1 s integration time. Monochromator slit widths for excitation and emission were set to a 5 nm band-pass. Excitation light fluctuations were corrected using a diode reference detector and all spectra were corrected PMT sensitivity. TCSPC measurements utilized a 341 nm pulsed LED light source (IBH) with a repetition rate of 500 kHz. Emission monochromators were set to a 3 nm band-pass and decays of each sample were taken with TAC range of 1 μs.

CHAPTER 3: RESULTS AND DISCUSSION

3.1. Independent Binding Site Model

To analyze the ITC data an independent binding site model commonly used for biological systems is used. This model is based on the chemical reaction depicted in equation 3-1 between a QD and a ligand, *L*.[39,61,64] Due to the competitive environment of TOPO and TOP being spectroscopically eliminated, it is safe to assume that QD-R_2Bts^{Me} interactions make up a vast majority of the chemical reactions described in this equation. For a sample of quantum dots with *N* surface sites per dot a series of equilibria can be written with their own corresponding equilibrium constants with *L* ligand:

$$QD + xL \leftrightarrow QDL + (x-1)L \qquad \text{[eqn. 3-1]}$$

$$QDL + (x-1)L \leftrightarrow QDL_2 + (x-2)L$$

$$\vdots$$

$$QDL_{N\text{-}1} + (x-N+1)L \leftrightarrow QDL_N + (x-N)L$$

Which is equivalent to a framework utilizing variable *j* for number of bound ligands:

$$QDL_{j\text{-}1} + xL \leftrightarrow QDL_j + (x-j)L \qquad \text{[eqn. 3-2]}$$

Within this framework, a QD macromolecule possesses *N* non-interacting binding sites assumed to each have the same intrinsic affinity for the ligand molecule. A general expression for the equilibrium constant for *j* bound ligand, K_j, is:

$$K_j = \frac{[QDL_j]}{[QDL_{j-1}][L]} \quad \text{[eqn. 3-3]}$$

At equilibrium the ratio of the forward, k^+, and reverse, k^-, reaction rates is constant, meaning that the j^{th} equilibrium constant can be written:

$$K_j = \frac{k_{j-1}^+}{k_j^-} \quad \text{[eqn. 3-4]}$$

Therefore, an expression can be determined through the Arhenius equation:

$$K_j = \frac{A}{B}\left(\frac{N+1-j}{j}\right) e^{-\frac{\Delta H_j}{RT}} \quad \text{[eqn. 3-5]}$$

In an independent binding site model ΔH_j, the enthalpy change, is not a function of j and is assumed to be constant. Therefore, from equation 3-2 an expression can be written for the concentration of quantum dots with j bound ligands utilizing an intrinsic site association constant, K_L, representing all constant variables:

$$[QDL_j] = \left(\frac{N+1-j}{j}\right) K_L [QDL_{j-1}][L] \quad \text{[eqn. 3-6]}$$

The site association constant, K_L, is related to the equilibrium constant for j bound ligand, K_j, by the following expression:

$$K_j = \frac{(N+1-j)}{j} K_L \quad \text{[eqn. 3-7]}$$

From equation 3-3, it is shown that K_L can be identified as the equilibrium constant for the reaction in equation 3-1 when $j = (N + 1)/2$.

In this model, expressions of total QD concentration, $[QD]_T$ (equation 3-8) and a concentration of ligand bound to a QD, $[L]_B$, for a particular QD concentration and free ligand concentration $[L]$ (equation 3-9) can be determined:

$$[QD]_T = [QD](1 + K_L[L])^N \quad \text{[eqn. 3-8]}$$

$$[L]_B = \frac{NK_L[QD]_T[L]}{(1+K_L[L])} \quad \text{[eqn. 3-9]}$$

However $[L]$ is not readily known, but can be written in terms of total ligand concentration, $[L]_T$, and concentration of bound ligand, $[L]_B$, where $[L] = [L]_T - [L]_B$. Some useful expressions can then be determined for the total concentration of bound ligand (equation 3-10) and for the sub-ensemble concentration of QDs with j bound ligands attached and N possible binding sites:

$$[L]_B = \frac{1}{2K_L}(1 + K_L[L]_T + NK_L[QD]_T \pm \sqrt{(1 + K_L[L]_T + NK_L[QD]_T)^2 - 4NK_L^2[QD]_T[L]_T}) \quad \text{[eqn. 3-10]}$$

$$[QDL_j] = \binom{N}{j} \frac{K_L^j [QD]_T ([L]_T - [L]_B)^j}{(1 + K_L([L]_T - [L]_B))^N} \quad \text{[eqn. 3-11]}$$

For each injection, the heat released or absorbed is given by:

$$Q = V\Delta H \Delta[L]_B \quad \text{[eqn. 3-12]}$$

Where V is the reaction volume, ΔH is the binding enthalpy, and $\Delta[L]_B$ is the change in bound ligand concentration. Equation 3-12 was used to fit the ITC isotherm data. A static quenching model for steady state PL intensity was also derived from the independent binding site model and is discussed later.

3.1.1. A Model to Include Two Ligands

From the inconsistent reproducibility present in this study, with samples or even an entire series of samples showing zero photoluminescence even with very little quencher added, it is a safe assumption that the R_2Bts^{Me} ligand does not work well as a primary passivating species. It appears that ligands such as TOPO, TOP, and HDA should be used for their exceptional passivating ability, followed by quencher ligand

exchange. TOPO would most likely allow ligand exchange easily as it has been shown to have a relatively weak site association constant.[39] The reason for this is due to the oxygen-cadmium bond being dative covalent. Since both of the electrons in the bond are donated from the oxygen atom, this creates a weak and curved bond in that hard-soft interaction. It is likely that other nucleophilic ligands would effectively compete against TOPO, allowing for ligand exchange within the system. Initial data that was gathered[61] from R_2Bts^{Me} ligand added to QDs with excess TOPO showed tangible heat interaction between quenching ligand and QD, as well as a more dramatic drop in PL intensity than what was observed from only adding TOPO to QDs, which supports the ability for ligand exchange to occur between R_2Bts^{Me} and TOPO.

Since desorption of TOPO would be possible in these systems, there would have to be a change in the model previously discussed in order to properly fit the isotherms in these hypothetical ITC experiments. The general chemical equation for the model would be slightly changed to account for TOPO desorption, where L_P would represent passivating ligand and i would be included as a variable describing amount of bound L_P. If we assume that for every quenching ligand bound a passivating ligand becomes unbound:

$$QD(L_P)_{i+1}(L)_{j-1} + xL + yL_P \leftrightarrow QD(L_P)_i(L)_j + (x-1)L + (y+1)L_P \qquad \text{[eqn. 3-13]}$$

Which then leads to an equilibrium expression for K_j:

$$K_{i,j} = \frac{A}{B}\left(\frac{N+1-(j+i)}{j+i}\right) e^{-\frac{\Delta H_j + \Delta H_i}{RT}} \qquad \text{[eqn. 3-14]}$$

Combined with a general expression for the equilibrium constant shown below:

$$K_{i,j} = \frac{\left[QD(L_p)_i(L)_j\right][L_p]}{\left[QD(L_p)_{i+1}(L_{j-1})\right][L]} \qquad \text{[eqn. 3-15]}$$

Yields an expression for the amount of QDs with *i* passivating ligands and *j* quenching ligands attached. The site association constant, K_L, is now accounting for intrinsic ΔH values of desorbing passivating ligand:

$$\left[QD\left(L_p\right)_i(L)_j\right] = \frac{\left(\frac{N+1-(j+i)}{j+i}\right)K_L\left[QD\left(L_p\right)_{i+1}(L)_{j-1}\right][L]}{[L_p]} \qquad \text{[eqn. 3-16]}$$

Where the sum of *j* and *i* are occupying the maximum amount of binding sites accessible on the QD, *N*. Since $i = N - j$ it is useful to make this substitution in order to decrease the number of variables. After this substitution expressions for $[QD]_T$ and $[L]_B$ can be determined:

$$[QD]_T = \sum_{j=0}^{N}[QD(L_P)_{N-j}(L)_j] \qquad \text{[eqn. 3-17]}$$

where:

$$\left[QD(L_P)_{N-j}(L)_j\right] = \frac{\left(\frac{N+1-(N-j+j)}{N-j+j}\right)K_L\left[QD(L_P)_{N-j+1}(L)_{j-1}\right][L]}{[L_P]} \qquad \text{[eqn. 3-18]}$$

which can be represented by a series of equations:

$$[QD(L_P)_{N-1}(L)_1] = \frac{\left(\frac{1}{N}\right)K_L[QD(L_P)_N][L]}{[L_P]}$$

$$[QD(L_P)_{N-2}(L)_2] = \frac{\left(\frac{1}{N}\right)K_L[QD(L_P)_{N-1}(L)_1][L]}{[L_P]}$$

$$\vdots \qquad \text{[eqn. 3-19]}$$

$$[QD(L_P)_{N-j}(L)_j] = \frac{\left(\frac{1}{N}\right)K_L[QD(L_P)_{N-j+1}(L)_{j-1}][L]}{[L_P]}$$

$$= \frac{\left(\frac{1}{N}\right)^j K_L^j[L]^j[QD(L_P)_N]}{[L_P]^j}$$

In an independent binding site model, the total QD concentration, $[QD]_T$ is usually known:

$$[QD]_T = \sum_{j=0}^{N}\left[QD(L_P)_{N-j}(L)_j\right] = [QD(L_P)_N]\left\{\sum_{j=0}^{N}\frac{\left(\frac{1}{N}\right)^j K_L^j [L]^j}{[L_P]^j}\right\} \qquad \text{[eqn. 3-20]}$$

Where $[QD(L_P)_N]$ represents the starting concentration of QD's in the sample before starting injections of quenching ligand. The total concentration of bound quenching ligand for a particular $[QD(L_P)_{N-j}(L)_j]$, free quenching ligand $[L]$ and free passivating ligand $[L_P]$ is determined by:

$$[L]_B = \sum_{j=1}^{N} j\left[QD(L_P)_{N-j}(L)_j\right] = \sum_{j=1}^{N}\frac{j\left(\frac{1}{N}\right)^j K_L^j [L]^j [QD(L_P)_N]}{[L_P]^j} \qquad \text{[eqn. 3-21]}$$

Unfortunately, yet another expression must be derived for the concentration of bound passivating ligand, $[L_P]_B$, as there are two ligands which are competing for QD binding sites, and therefore the distinction of passivating ligand available in solution is key. Keeping the assumption that the initial sample has all QDs saturated with passivator and that a passivator must desorb before a quencher can adsorb:

$$[L_P]_B = \sum_{j=0}^{N}(N-j)\left[QD(L_P)_{N-j}(L)_j\right] = \sum_{j=0}^{N}\frac{(N-j)\left(\frac{1}{N}\right)^j K_L^j [L]^j [QD(L_P)_N]}{[L_P]^j} \qquad \text{[eqn. 3-22]}$$

From this point simplifying the above expressions would be useful in order to more easily express $[L]_B$ and $[QD]_T$ and $[L_P]_B$ in terms of known quantities. From that point the next step would be to substitute the free ligand concentrations $[L]$ and $[L_P]$ for $([L]_T - [L]_B)$ and $([L_P]_T - [L_P]_B)$. This would then allow for all expressions to be in terms of known quantities $[L]_T$, $[L_P]_T$, $[QD]_T$, and values that can be solved for/approximated N and K_L. Future studies that have a more prevalent amount of passivating ligand might benefit from this basis for a two-ligand model.

3.2. General Characterization of R_2Bts^{Me}

Cyclic voltammetry (Figure 3.1) and ^1H NMR spectra (Figure 3.2) were obtained of the three R_2Bts^{Me} ligands. The cyclic voltammetry (CV) scans for all R_2Bts^{Me} species showed a consistent chemically irreversible process, causing an $E_{1/2}$ calculation to be impossible. Instead, the differences between each ligand oxidation and the $E_{1/2}$ of ferrocene standard were found. These values at least give some clue toward the relative HOMO energies for each R_2Bts^{Me} species. Similar to what was found in a previous study,[61] the relative HOMO energies in descending order are Et_2Bts^{Me}, Me_2Bts^{Me}, and Ph_2Bts^{Me}. Phenyl groups are capable of electron withdrawal depending on the species to which it is attached.[104] The resonance possibilities for an aromatic group allow it to serve either as an electron donating substituent when the attached atom needs electrons (carbocation) or as an electron withdrawing substituent when the attached atom has a lone pair to share (such as with sulfur, oxygen, or nitrogen). It was assumed that the phenyl groups in this study would be electron withdrawing due to the presence of lone pairs on the sulfurs.

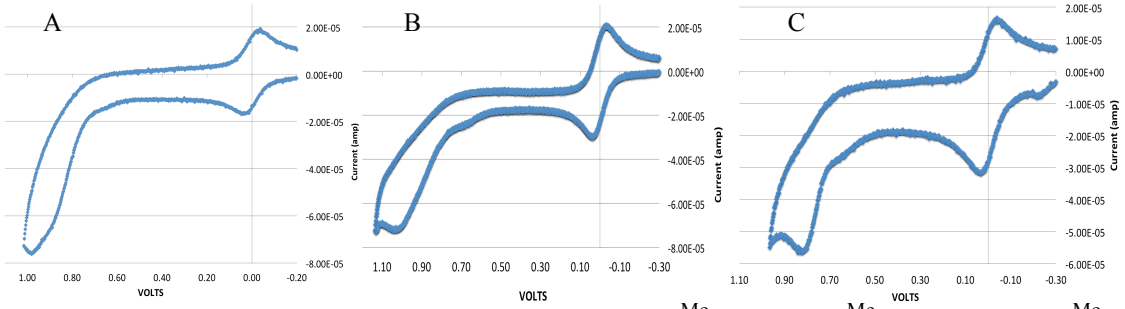

Figure 3.1: Cyclic voltammetry scans for A) Me_2Bts^{Me}, B) Et_2Bts^{Me}, and C) Ph_2Bts^{Me} using a graphite electrode and tetrabutylammonium hexafluorophosphate ($TBAPF_6$) as the electrolyte in acetonitrile solvent at a scan rate of 200 mV/s with a ferrocene standard present. The differences between ligand oxidation and $E_{1/2}$ of ferrocene were found to be A) 0.98 V, B) 1.03 V, and C) 0.82 V.

It can be determined from the combination of CV and ^1H NMR scans that the

phenyl groups present in the Ph_2Bts^{Me} compound are electron withdrawing relative to the related methyl and ethyl species, which was a subject of great debate until this data was obtained.

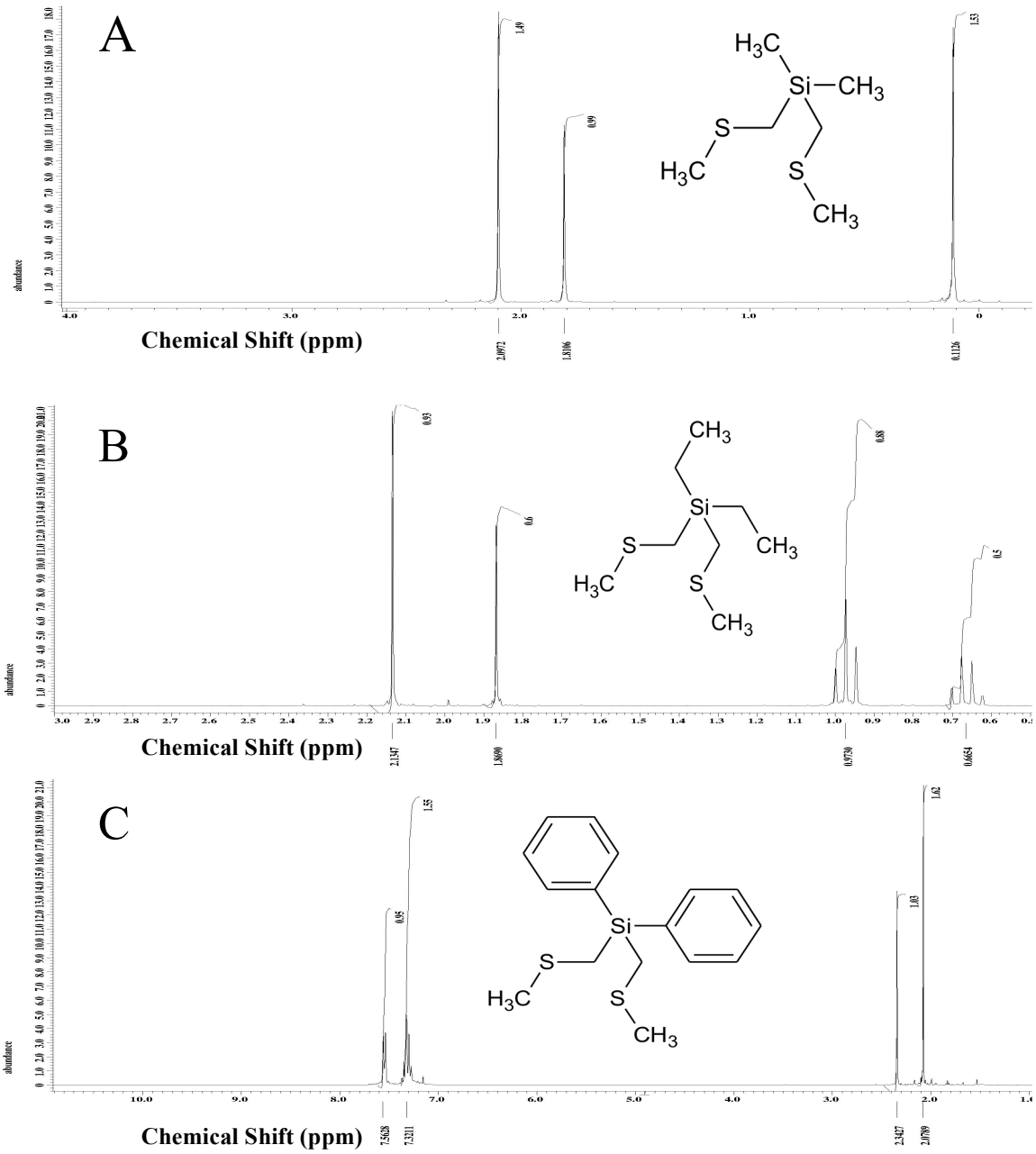

Figure 3.2: ^{1}H NMR spectra of A) Me_2Bts^{Me}, B) Et_2Bts^{Me}, and C) Ph_2Bts^{Me} in $CDCl_3$ solvent with corresponding molecular structures shown.

The ^{1}H NMR spectra give some insight into whether the phenyl groups in the Ph_2Bts^{Me} compound are indeed electron withdrawing. Though the phenyl functional groups are electron-rich, it can be observed that there is a shift downfield in the methylene group to 2.34 ppm, while the same methylene proton position in the Me_2Bts^{Me} and Et_2Bts^{Me} compounds are shown to be at 1.81 ppm and 1.87 ppm, respectively. This shift in itself is not enough evidence to support the idea that the phenyl groups are electron withdrawing. However, we can further examine the position of each methylene peak relative to the peak corresponding to the methyl groups located at the end of each thioether chain. For the Me_2Bts^{Me} and Et_2Bts^{Me} compounds we see the peaks representing the terminal thioether methyl groups located furthest downfield. For the Ph_2Bts^{Me} compound, we see that the peak corresponding to the methylene groups is shifted more downfield than the peak for the terminal methyl groups. The terminal methyl groups are too far away to receive deshielding effects from the electron withdrawing phenyl groups. The methylene groups are directly attached to the central silicon atom, therefore capable of being deshielded by the phenyl groups.

3.3. Photoluminescence Measurements

PL measurements were taken at equilibrium for the Et_2Bts^{Me} and Me_2Bts^{Me} species. A full explanation of all PL effects while the system has yet to reach equilibrium is beyond the scope of this work and would require time dependent experimental methods to be run.

3.3.1. Steady-State Measurements

A model to fit steady state photoluminescence data was developed utilizing the assumption that static quenching was occurring. In this model it is assumed that only

QDs with no quenching ligands attached are capable of fluorescing. Therefore, a function can be derived from equation 3-8 where $j = 0$ and PL intensity, I, is proportional to $[QD]$:

$$I\ \alpha\ [QD] = \frac{[QD]_T}{(1+K_L[L])^N} \qquad \text{[eqn. 3-23]}$$

This means that I is equal to a constant, c, multiplied by $[QD]$, and while there is no way of knowing $[L]$, the concentration of free ligand in solution, we can write it in terms of $[L]_B$, the concentration of bound ligand, and $[L]_T$, the total ligand concentration, knowing that $[L] = [L]_T - [L]_B$.

$$[QD] = \frac{[QD]_T}{\left(1+K_L([L]_T-[L]_B)\right)^N} \qquad \text{[eqn. 3-24]}$$

Where $[L]_B$ can be determined by using equation 3-10. Figures 3.3 and 3.4 illustrate raw steady state photoluminescence data and data fit using the above function.

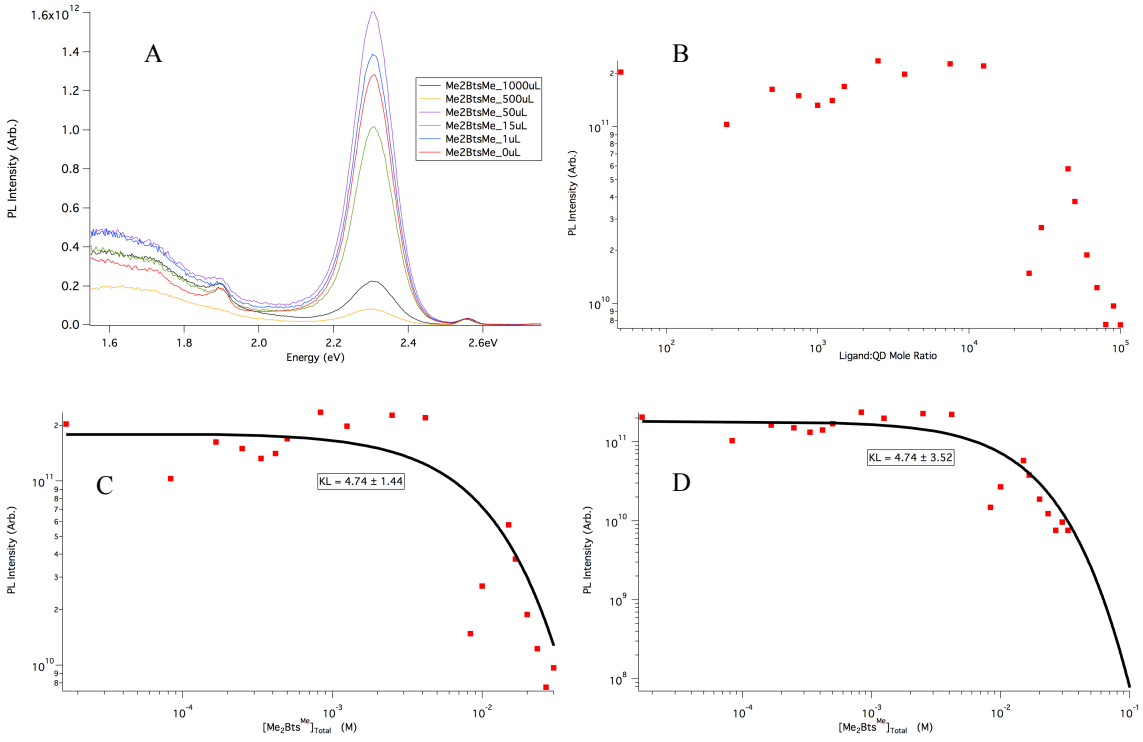

Figure 3.3: Raw PL intensity of QDs with Me_2Bts^{Me} incrementally added is shown in (A). Integrated areas of Photoluminescence intensity plotted as a function of ligand:QD

molar ratio is shown in (B). These integrated peaks were then plotted vs. total concentration of Me_2Bts^{Me} and fit using equation 3-24 in both (C) and (D). A fit with an expanded x-axis range was attempted for (D) in order to explore further behavior of the fit function.

The fit of the above data yielded a value for the site association constant, K_L, of 5.676 M^{-1}. This value is smaller than the site association constant found in a previous work for TOPO.[39] It is important to realize that the site association constant for the Me_2Bts^{Me} species is very low, and supports that TOPO binds approximately six times more readily to CdSe surface. This is an unexpected value, as it was hypothesized that the sulfur, a relatively strong nucleophile, would strongly bind to cadmium, a good electrophile.

It was most likely an effective method to wash the QD stock until ^{31}P NMR showed only background noise, as a QD stock solution with excess TOPO present would have made it difficult to see any effects from the addition of Me_2Bts^{Me} ligand.

A result like this also explains why gathering consistent data from experiments involving the ITC was so difficult. It was a challenge obtaining usable data showing thermodynamic trends associated with the incremental addition of Me_2Bts^{Me} into QD solution. If there was very little binding interaction occurring, as supported by the above K_L value, then this would lead to very minor heat exchange in the system.

Expansion of the x-axis was also done to examine the behavior of the fit function beyond the limit of the data. This did not yield much of a difference and simply showed that the fit function would continue to decrease in a downward curvature. The function eventually developed an index point in its attempt to continue to fit the data points and also incorporate the rest of the independent value range. It was not expected that the

fitting function would tail off at a constant minimum, as it did not have an expression designed to show such behavior.

This study explored rather large concentrations of R_2Bts^{Me} relative to the concentration of QDs, and the fact that there was no minimum reached for the QD PL supports two main possible points: (a) The QD surface is saturated with passivating ligand to the point where the weaker binding quencher can no longer adsorb to the surface, or (b) the surfaces of the QDs were damaged to the point where acceptable binding sites were limited. There were some samples and in fact one entire series each of Et_2Bts^{Me} and Me_2Bts^{Me} that showed zero photoluminescence even with no quenching ligand added. For the entire series that showed no PL intensity, it was later found that there was an air leak in the flask where the QDs were stored. This would allow for the QD surfaces to become oxidized and destroyed. Surfaces of QDs which are badly damaged are highly unlikely to fluoresce, whether there is quenching ligand present or not. In the cases where the occasional individual sample would yield little to no PL, most likely it is a hidden scenario "c" that effectively explains this result. Due to low R_2Bts^{Me}-QD interaction, evident from the low K_L value, inconsistencies can happen. It is far more likely that a sample of cleaned QDs were not dispersed well in hexane solvent as there was not enough passivation occurring. Relying on the R_2Bts^{Me} compounds to passivate the QDs and allow them to break apart from their clusters to fluoresce is not consistent, especially when not in heavy excess.

Similar steady state PL tests were done on two series where Et_2Bts^{Me} was added to solutions of CdSe quantum dots. A second series was done to more effectively show PL quenching through a slight adjustment of the ligand:QD molar ratio.

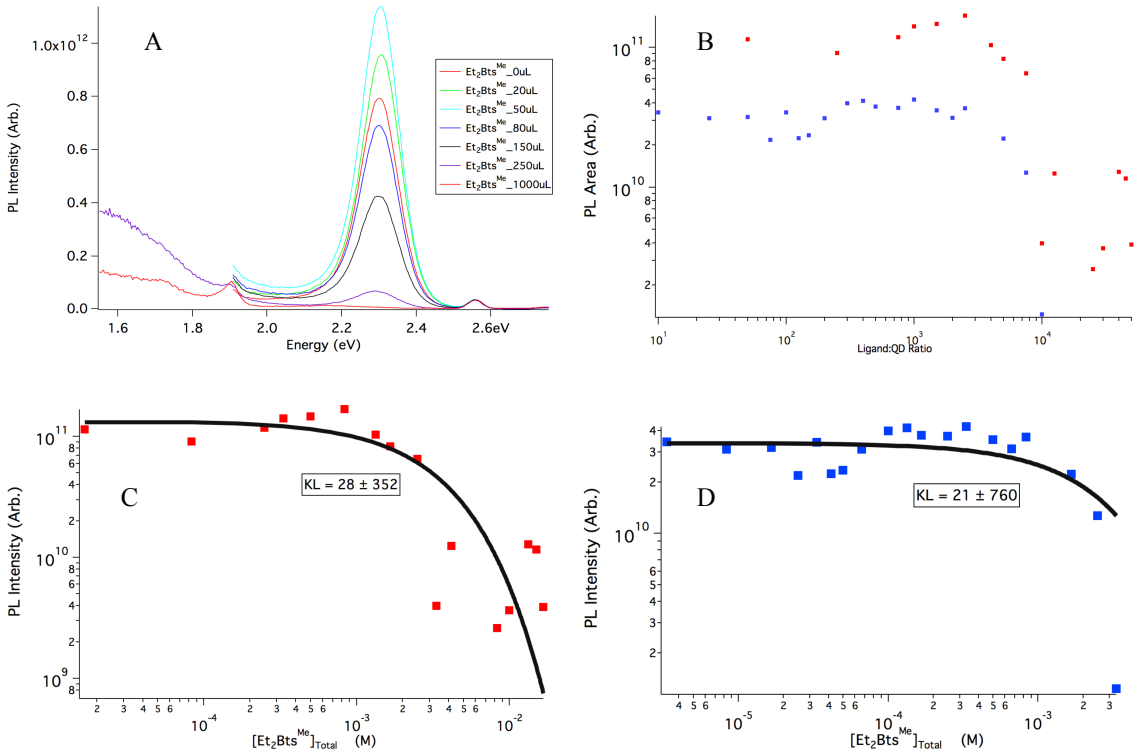

Figure 3.4: Raw PL intensity of QDs with Et_2Bts^{Me} incrementally added is shown in (A). Integrated areas of two series of QD-Et_2Bts^{Me} solutions are plotted vs. Ligand:QD mole ratio in (B). In (C) and (D), integrated PL of these two series is plotted vs. total concentration of the Et_2Bts^{Me} species and fit using equation 3-18.

These data show a site association constant for Et_2Bts^{Me} averaging 23.5 M^{-1}. This value is slightly weaker than the value found for TOPO[39] but is about five times greater than what was found for Me_2Bts^{Me}. This result would imply that the Et_2Bts^{Me} species is more consistent, and indeed it was. It was far easier to obtain reproducible data in both PL studies and ITC experiments. Again, there was no minimum to the PL intensity reached despite these series ending in high ligand amounts, supporting that the QDs had their binding sites occupied by TOPO ligand, limiting the amount of quencher that could adsorb to QD surface.

3.3.2. Similarity to the Stern-Volmer Model

The static quenching function used in this work is similar to the static quenching Stern-Volmer model introduced in Chapter 1, where a linear relationship for the ratio $\frac{I^0}{I}$ was dependent upon an association constant, K_{sv}, and total concentration of quencher, [Q]. There are however two key differences between the models used in this study and the Stern-Volmer model. Stern and Volmer used systems where there was only one possible chemical reaction between surface and quencher, and this allowed them to only consider total concentration of quencher. In our case, QDs have multiple binding sites available for ligands to bind once introduced into the solution. A system like this requires a variable representing the many binding sites on the QD surface, *N*, and also a distinction between free ligand in solution, bound ligand, and total ligand concentrations [L], $[L]_B$ and $[L]_T$, respectively. While the Stern-Volmer plot is $\frac{I^0}{I} = 1 + K_{sv}[Q]$, our quenching model, when adjusted to the ratio of original PL intensity, I^0, divided by PL intensity with quenching ligand added, *I*, simplifies to:

$$\frac{I^0}{I} = \frac{[QD]_T}{(1+K_L*0)^N} * \frac{(1+K_L[L])^N}{[QD]_T} = (1 + K_L[L])^N = \left(1 + K_L([L]_T - [L]_B)\right)^N \qquad \text{[eqn. 3-25]}$$

The close relation between the two models is easily observable. The quenching phenomenon for our study does however exponentially increase with *N* binding sites. The model also distinguishes between the concentration of free ligand [L] instead of total ligand concentration, $[L]_T$ or [Q]. In both cases the function is plotted versus total ligand concentration as shown in figures 3.5 and 3.6.

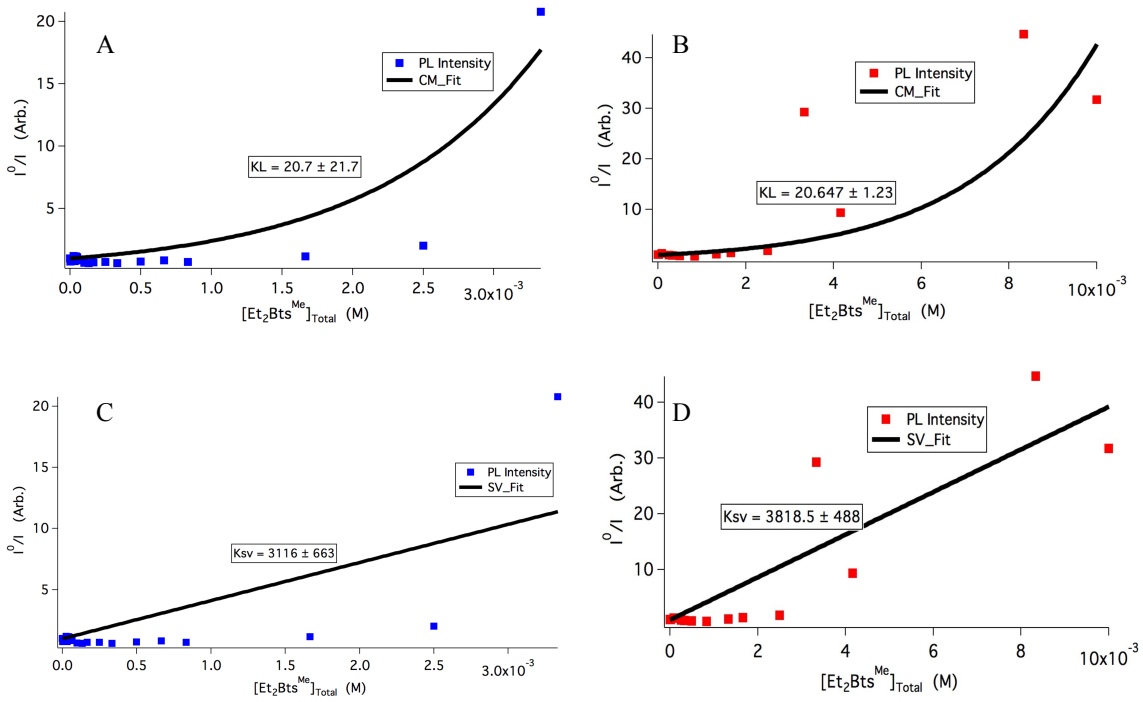

Figure 3.5: Two series of steady state PL measurements showing PL change as a function of total Et_2Bts^{Me} ligand added is shown. (A) and (C) show the first series fit using the quenching model used in this study and the Stern-Volmer model, respectively. (B) and (D) depict the second series of data in similar fashion.

It is clear that the Stern-Volmer quenching model does not fit the data, and requires consideration of added variables as a linear model seems inadequate. In these plots that mimic the Stern-Volmer method, it is worth noting that N and K_L were highly correlated. For the Et_2Bts^{Me} species there seems to be a major change in the solution at $3x10^{-3}$ M. It is at this point that I^0/I deviates considerably, showing the moment when PL intensity is greatly decreased. This appears to be the critical concentration in which many QDs become affected by the quenching capabilities of the species. Since the K_L values between the trials are similar this lends confidence to the analysis of this system using the independent binding site model. The following figure shows a series of steady state PL data taken for the addition of Me_2Bts^{Me} fit mimicking the Stern-Volmer method, and it shows the same overall result.

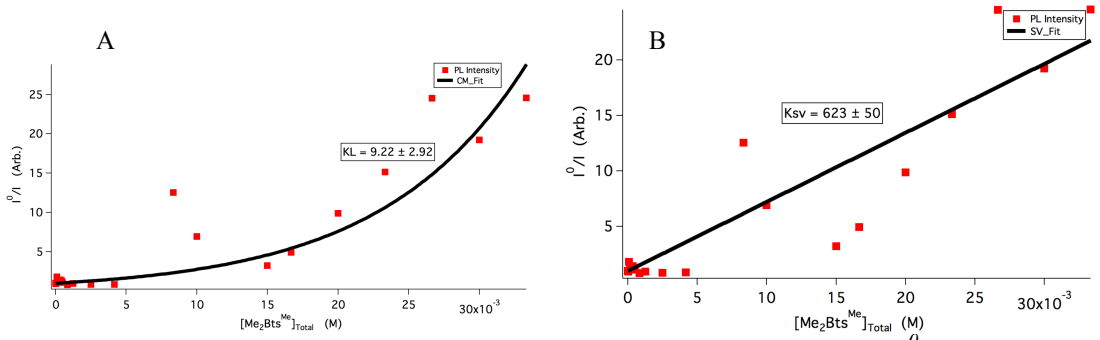

Figure 3.6: A single steady state photoluminescence series depicting I^0/I as a function of added Me_2Bts^{Me} is shown, fit using the quenching model from this study in (A), and the Stern-Volmer model in (B).

For these data the initial points where very little quencher was added is fit much better using the model shown in (A). The Stern-Volmer model does not properly fit four of the low-concentration data points. This serves to further portray the exponential factor associated with these data.

3.3.3. TRPL Measurements

Time-Resolved photoluminescence data was collected and parameters determined via least squares fits using home-built software for Et_2Bts^{Me} and Me_2Bts^{Me}. The data shows that there is little difference between the PL lifetimes of systems with no ligand added and systems where a high concentration of ligand was added, in fact showing increases in lifetimes as ligand is first introduced to the systems. This is shown in figure 3.7.

From a plot of average PL lifetimes as a function of total ligand concentration it was determined that static quenching for this system was a safe assumption. In a system where static quenching is occurring, PL lifetimes will show no trend, as the only QDs that fluoresce are QDs with no quenching ligand attached. A system where QD PL lifetimes steadily decrease would support dynamic quenching. This is due to the fact that

dynamic quenchers do not separate charge as efficiently as static quenchers, and therefore the radiative pathway of the exciton is still accessible. As more dynamic quenchers adsorb to the QD surface, the less chance an exciton can recombine radiatively, until only the fastest radiative lifetimes are able to compete against the many ligand-induced charge transfer pathways.

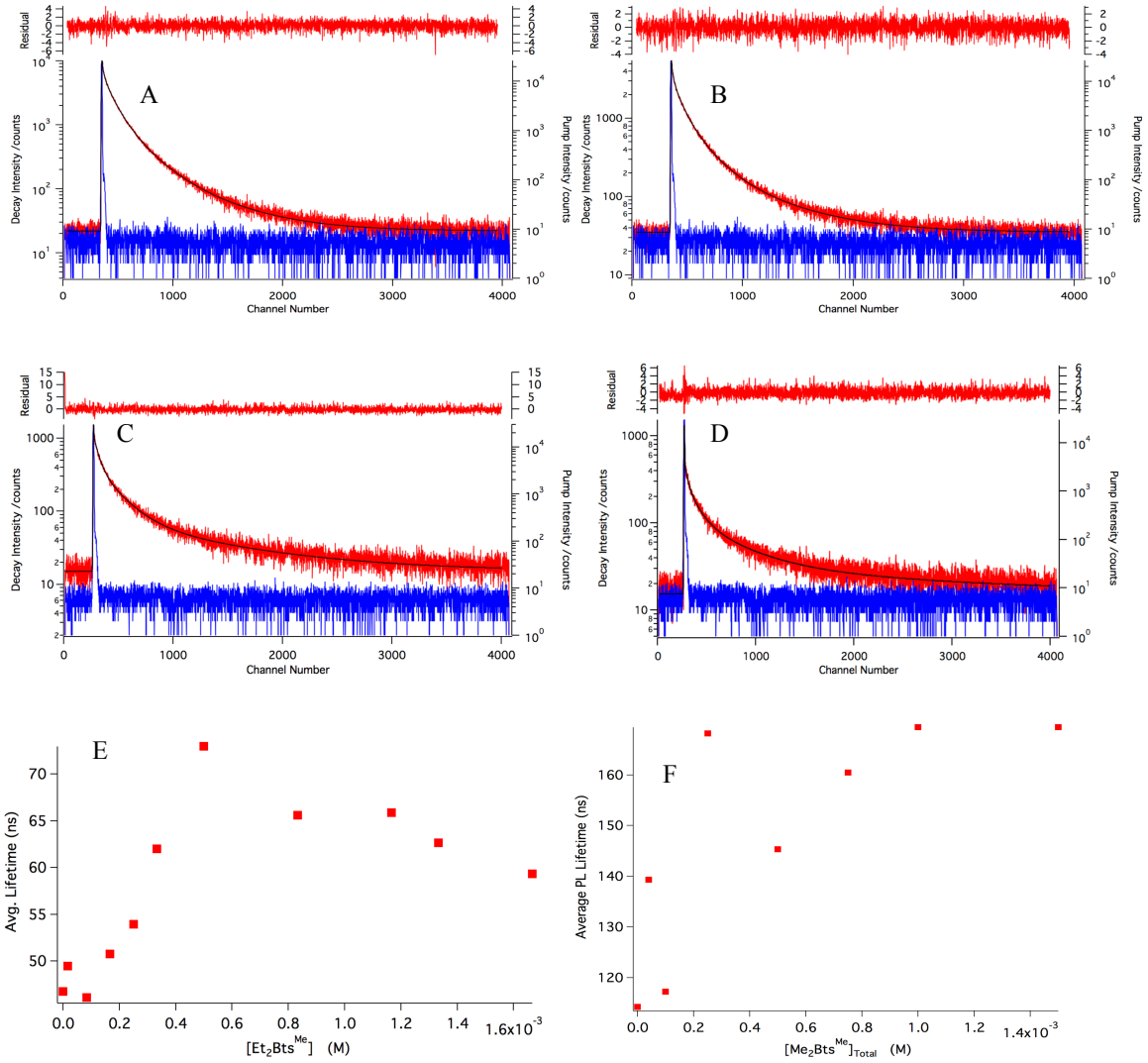

Figure 3.7: PL Lifetimes are shown for QD systems with no Et_2Bts^{Me} added (A) and with a total concentration of 2 mM Et_2Bts^{Me} present (B). Parts (C) and (D) show lifetimes for the same concentrations of Me_2Bts^{Me} added. The average lifetimes are plotted vs. total ligand concentration for each series of systems is shown in (E) and (F).

The plots in figure 3.7 show a rise in average lifetime before steadying. This

initial rise in lifetimes is most likely due to disaggregation of QD clumps. The newly freed QDs would then be able to fluoresce, which would lead to an increase in quantum yield and lifetimes. As concentration of quencher increased, the disaggregated QDs became properly quenched which then lowered average lifetimes and quantum yield until lifetimes became generally constant. Figure 3.8 shows the close correlation between quantum yield and lifetimes for Et_2Bts^{Me}.

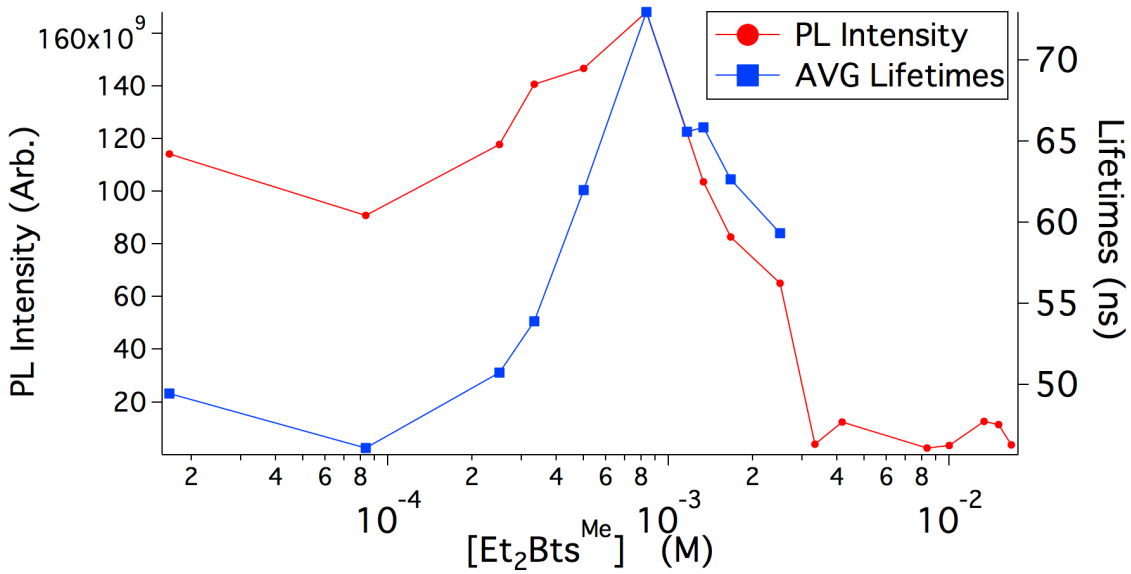

Figure 3.8: Average lifetimes in nanoseconds for a sample of Et_2Bts^{Me} in QD solution are shown in blue and follow the right y-axis. PL intensities for the same sample with extra points of increased concentrations are shown in red and follow the left y-axis under arbitrary units. Both variables are plotted as a function of Et_2Bts^{Me} concentration.

3.4. ITC Measurements

Measurements for Et_2Bts^{Me} and Me_2Bts^{Me} were taken using isothermal titration calorimetry in incremental titrations, where the amount of heat required to keep the sample and reference cells fixed to the same temperature was determined for each injection. The system was allowed to return to equilibrium after each injection.

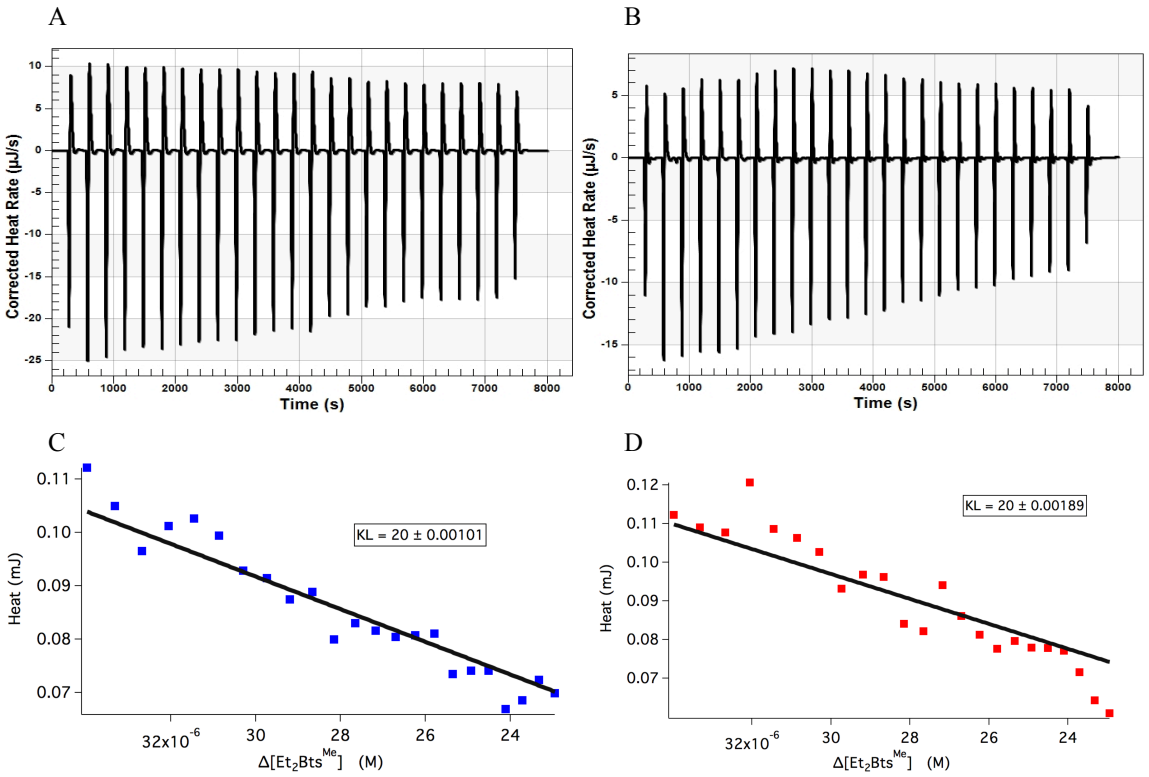

Figure 3.9: Raw ITC data depicting heat with baseline subtracted as a function of time is shown for (A) Et_2Bts^{Me} and (B) Me_2Bts^{Me}. Parts (C) and (D) show integrated heats as a function of changing Et_2Bts^{Me} concentration.

The data obtained from the ITC was fit using equation 3-12, with K_L values at 20 M^{-1}, close to the values found from the steady state PL fits. The data presented here does not however show a plateau, or a point where heat exchange remains relatively constant per injection. This shows that unfortunately the QDs in the sample cell were not fully saturated, as reactions appeared to still be occurring by the end of the experiments. Since the ITC at UNC Charlotte is specifically designed for low volume work, there is little volume in the titration syringe to work with, which makes it difficult for a system to become saturated to the point where heating plateaus occur. The limited volume combined with the fact that each ligand has a low association constant makes it an even more prevalent challenge to saturate QDs with the R_2Bts^{Me} species. By Le Chatelier's principle injecting more ligand should still drive a reaction to a saturated equilibrium

despite low association strengths, however this would require a very concentrated solution to be present in the titration syringe. ITC runs that were done with Et_2Bts^{Me} yielded noticeably more consistent trends than the Me_2Bts^{Me} compound. This does make sense, as association constants for Et_2Bts^{Me} were about five times higher than for Me_2Bts^{Me}. This supports the idea that reactions were happening consistently more often for Et_2Bts^{Me} than Me_2Bts^{Me}. To achieve ITC data that boasts a heat exchange plateau, a ligand with a higher affinity for CdSe surface would more easily saturate the QDs in the sample cell. Hopefully the limited titration volume would then be enough to develop a more complete set of ITC data.

3.5. ITC Difficulties

Throughout over a year of obtaining ITC data, there were many obstacles that presented themselves. The first problem was taking care to obtain preliminary results that signify the ITC is ready for use. This is typically done through scans where solvent is titrated into more pure solvent. The peaks that follow each injection should be exothermic and with an area between 1 μJ and 5 μJ. Using isopropanol this was done easily. However, after transitioning the ITC to hexane solvent, results became more difficult to interpret. Figure 3.10 illustrates the differences between these solvent into solvent control scans. In order to have some stability in the hexane system, cells were overfilled to 750 μL. For the first several injections, small exothermic peaks can be observed, which show the ITC is ready for experimental scans using hexane solvent. The strange behavior present in the rest of the control scan can be explained when you consider the high vapor pressure of hexane. The platinum covered shaft that connects the sample cell to the chamber that houses the buret handle is very narrow. Pure hexane

evaporates very quickly once it enters this shaft, and it does not take long for the hexane level to reach the sample cell. Once this happens, any form of thermal stability is lost. For these control scans I would suggest overfilling into the well of the ITC to provide more time before the strange peak behavior occurs. Solutions that use hexane as a solvent but contain less volatile components are much more stable than pure hexane, and therefore overfilling the sample cell with only 200 μL was sufficient for an entirely stable scan.

The original system implemented for the ITC experiments were CdSe/CdS core-shell QDs passivated with excess TOPO. Good ITC experiments require a fine-tuning of concentrations between titrant and sample. As shown in figure 3.11, the heat isotherms between Me_2Bts^{Me} titrated into the QD sample and the same ligand titrated into hexanes are nearly identical. In the control runs where there is no possibility of binding interaction, heat transfer occurs from diffusion and dilution. Since there was negligible difference between the control scans done and the scans that involved sample, it appeared that there was no tangible binding interaction occurring between added ligand and QD.

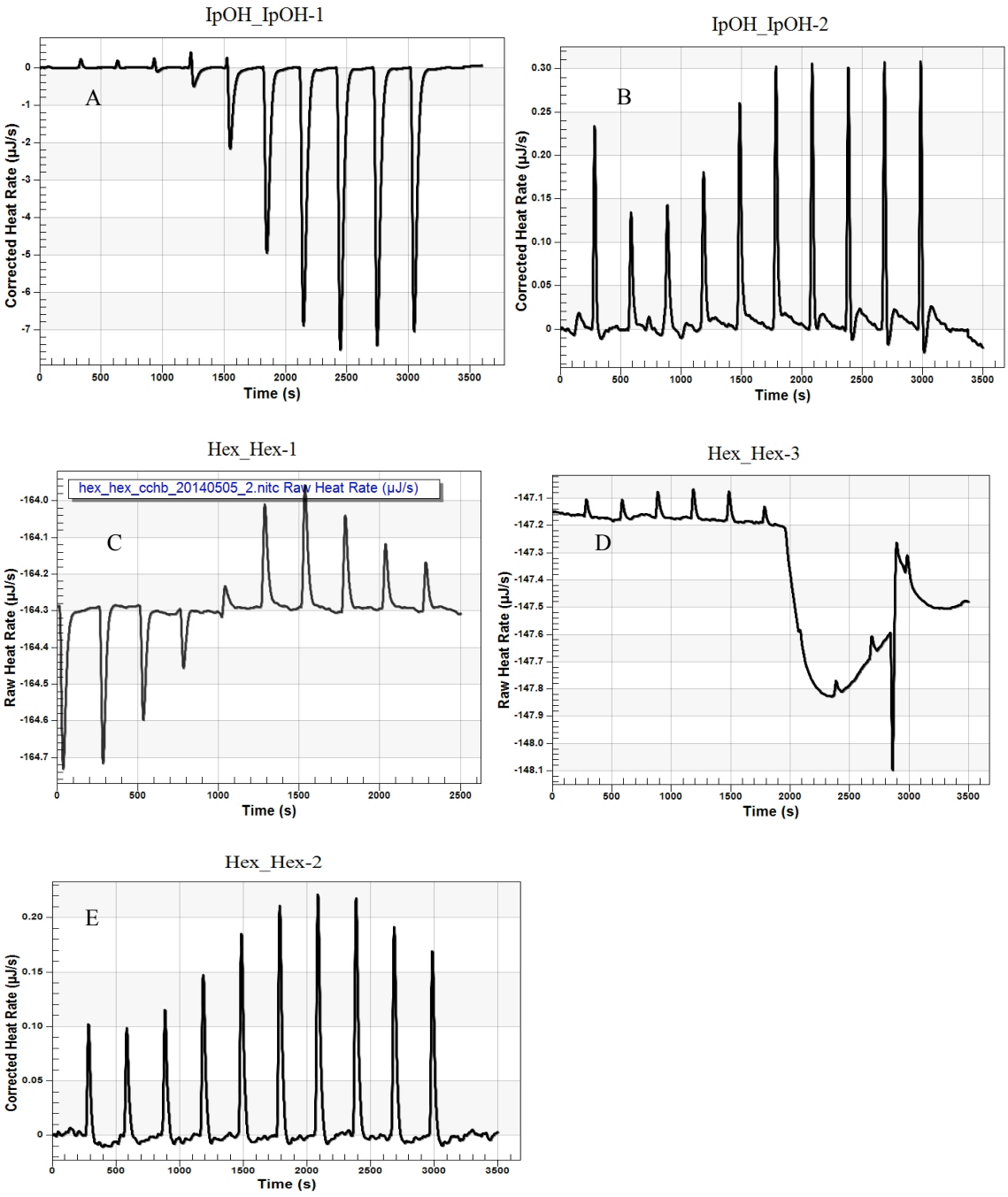

Figure 3.10: Titrations of solvent into solvent are shown for isopropanol in A and B and for hexane in C, D, and E. The scan shown in A reflects a sample cell not yet fully cleaned therefore causing other endothermic types of heats to occur. Scan B shows a fully cleaned sample cell. C depicts a sample cell that was not properly adjusted to organic solvent and showing a transition between endothermic dilution heat to exothermic diffusion heat. The scan in D shows a sample cell that has been properly cleaned and equilibrated, but evaporation of hexane eventually leads to the strange instrument behavior at approximately 2000 seconds. The scan shown in E illustrates a properly cleaned and equilibrated instrument with extra hexane added to the sample cell.

The experimental concentrations of the solutions involved should also be addressed. For the first scans, the concentration of ligand was 0.125 M. For an ITC model that specializes in low volume work this is a very large concentration, yet there was no tangible binding. The QD solution had a concentration of approximately $5x10^{-9}$ M, a very low concentration in a solution with excess TOPO. The QDs had to be replaced by another set of QDs that were not as saturated, and in a higher concentration to provide more interaction. A fresh sample of CdSe core QDs was then made and put into sample solutions with concentrations approximately $5x10^{-7}$ M. This concentration of QDs as well as the fact that ligand concentration was increased to 0.5 M helped establish some difference in isotherm data for ligand titrated into QD experiments and ligand titrated into solvent control scans. Later the stock QDs that were made were washed twice using acetone to spectroscopically eliminate presence of TOPO and TOP using ^{31}P NMR. This was done in an attempt to simplify the system inside the ITC to more accurately model the data.

It was originally thought that the extremely high ligand concentration was also detrimental to the ITC data, and that such a high concentration was causing exothermic "rebound" peaks to occur. Concentration of the ligand titrant was then decreased greatly to 5 mM. This appeared to work relatively well for the Et_2Bts^{Me} species but the Me_2Bts^{Me} species did not seem to show tangible binding interaction. This later made sense after their corresponding K_L values were determined. The site association constant for Me_2Bts^{Me} was so small that it would have taken an extremely large concentration in order to show binding interaction in the ITC.

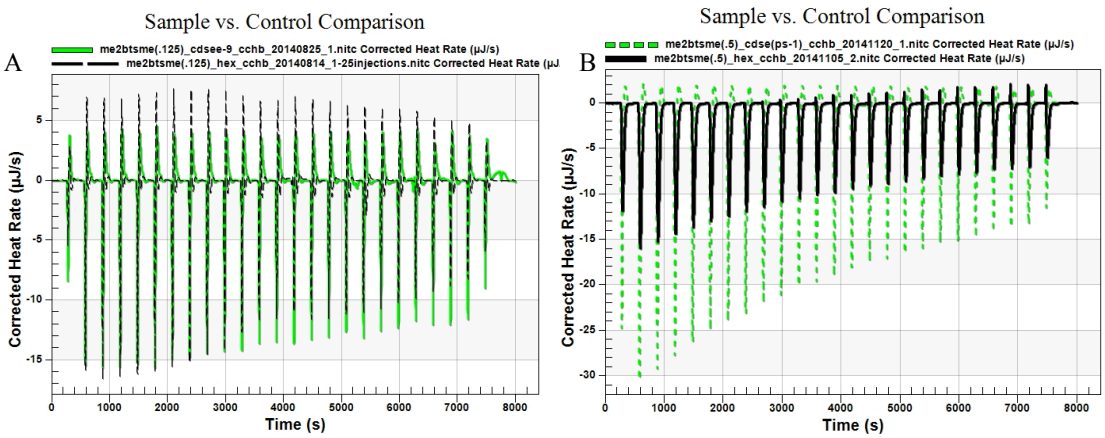

Figure 3.11: Comparison scans of sample experiments vs. control scans are shown. In A, the green data represents Me_2Bts^{Me} titrated into a solution of CdSe/CdS core-shell QDs dispersed in hexane solvent. The black data represents a control scan of the same ligand titrated into hexane. The peaks are comparable in magnitude and area with no distinct trend in difference. Part B shows a similar comparison, where black shows the control scan and green shows the sample run. There is a clear difference in peak magnitudes between the experiments. Changing the QD concentration by two orders of magnitude and the ligand concentration to 0.5 M appeared to help achieve the difference shown in B.

Following this issue the question arose as to why there were "rebounding" peaks that immediately followed the peaks showing proper isotherm behavior. Most likely this anomaly is due to the fact that the instrument is specially designed and calibrated for aqueous solutions. In the advanced settings of the instrument software there is a setting called "compensation." The compensation refers to the amount of power required for the instrument to keep the difference in temperature between the sample and reference cells zero. This setting should not be changed, as any slight change to the compensation causes the windows that monitor the behavior of the instrument to oscillate and vary with high magnitudes of difference, even when the instrument is idle. The instrument response rate should be considered constant for your experiments as long as the same solvent is used throughout. If the isotherm peak areas dominate the constant unwanted peak areas consistently then it should be acceptable to integrate each injection entirely.

There may still be the possibility of calibrating the instrument for organic solvent, though the process takes many days and was not something I was able to properly accomplish. The rebounding peak is actually more common than originally thought, as ITC models that require larger volumes also have them. The experiments for these ITC models however tend to have much higher heat interactions and magnitudes, which make the rebound peaks less noticeable. With an ITC that specializes in low volume work and therefore very small heats, the area around the baseline is much more highlighted. It is my opinion however that it is okay to use very large concentrations of titrant in order to achieve a plateau where further injections only lead to diffusion and dilution heat interaction rather than binding interaction. With such a small titrant volume to work with, I urge my successors on the ITC to not hesitate to use large concentrations of ligand in order to achieve full and complete ITC isotherms. This can be difficult when only 50 μL of total titrant are available.

There is one more thought about the low volume ITC that I have and that is in the set up window on the software there is a small setting that allows the operator to choose what the expected heat magnitudes will be: small, medium, or large. Throughout this research project that setting of expected heats was always set to "small," and perhaps rightfully so. However, changing of this setting may be required depending on how the operator would like to specialize the ITC toward his or her system.

There was some issue regarding whether or not the peaks shown from the ITC experiments were endothermic or exothermic. Depending on the type of calorimeter that is used, both directions (positive or negative) can apply to endothermic or exothermic interaction. This was the cause of much debate, and it was eventually determined by

special experimental design that for this instrument a peak in the negative direction was endothermic and peaks in the positive direction were exothermic. There are two ways that this can be determined. The first is fairly straightforward and it is to perform a titration of solvent into solvent. With only diffusion heat being transferred, injections should lead to small exothermic peaks. Whichever direction (positive or negative) the peaks extend would be the exothermic direction. For further proof, another general solvent into solvent titration can be done, using a heated titrant. After each injection the elevated temperature disperses outward toward the surroundings, imitating an exothermic reaction. Whichever direction the peaks take during this experiment should provide the exothermic direction. Some solvents are more volatile than others, such as hexane or pentane. For these types of solvents it may be beneficial to cool the titrant rather than heat it and imitate endothermic reaction conditions. In this case the peaks should point in the endothermic direction.

3.6. What the Results Mean for the Independent Binding Site Model

The results from this experiment show that there is some merit in using the independent binding site model for projects involving QD charge transfer dynamics. Unfortunately, a full series of data showing ITC and PL behavior for all three R_2Bts^{Me} ligands was not possible. From the data that can be presented, it seems that the association constants from the ITC modeling agree closely with association constants obtained from the PL static quenching models that were derived from the independent binding site model. The static quenching model appears to fit the data rather well, and this supports that the independent binding site model is viable in a regime where only one ligand needs to bind in order to quench photoluminescence. The single ligand that binds

is binding independently as it is the first quencher that adsorbs to the QD surface.

CHAPTER 4: CONCLUSIONS

4.1. R_2Bts^{Me} Quenching Conclusions

It has clearly been shown that the R_2Bts^{Me} species is capable of quenching in this study and one done previously that did not solely focus on a QD-R_2Bts^{Me} system.[61] TRPL data supports that these ligands statically quench QD photoluminescence with differing site association constants. Unfortunately, time constraints have severely limited the comparison of these three compounds. To improve the issue of time problems, starting with a more stable system is essential for reproducible results. It stands to reason that attempting tests on QDs not originally well passivated will yield inconsistent results when the ligand of interest does not boast a long carbon chain capable of stabilizing the QDs in colloidal suspension nor a strong site association constant. A better starting point should provide consistent results and this can be done by allowing QDs in stock solution to be well passivated with TOPO, rather than left dry with little TOPO present, as was done in this study. Expanding upon the model that includes two ligands with different roles would allow for more accurate fit functions for future experiments using these types of systems. Other types of ligands, such as thiones or thiols, should perhaps be used instead of the R_2Bts^{Me} species, as they may be able to bind more strongly to QD surface and compete with the TOPO passivators.

4.2. Independent Binding Site Model Conclusions

Use of the ITC in conjunction with PL and TRPL studies is a type of work still in

its infancy, as very few organic QD systems have been studied using this technique. The ITC provides a method for the direct measurement of thermodynamic parameters resulting from the binding of ligands to QDs, values previously only attainable through Langmuir models to fit PL quenching data. The ITC provides a means of determining these values with greater accuracy since it directly measures the thermodynamics of a system, and also a ligand's effect on PL does not affect the capability of the ITC to determine binding parameters. Unfortunately, using this model does not allow for the finding of independent values for ΔH and N (the number of binding sites available on the QD surface) as these variables are tightly correlated when performing fits for the data. As one changes, the other adjusts proportionally, leading to an inability to separate the values for these two variables. One way that these two variables could be differentiated is by performing ITC scans of each system at different operating temperatures. This would allow for determination of parameter differences dependent on temperature, hopefully exposing an enthalpy of ligand-QD interaction per injection.

The independent binding site model should be adjusted to include the enthalpy associated with desorption of passivating ligands. Once this is done a more accurate determination of the number of ligands bound to the QD surface would be possible for a system that has two competing ligands present. This will then lead to a better idea of the probability of charge transfer to a ligand.

ITC is an old technique[64] used for many years by biochemists experimenting on aqueous systems, and has recently started being used for novel QD-ligand systems[39,61,69] allowing for direct characterization of the thermodynamics of QD-ligand interactions. Results and the application of data obtained using this technique shows promise.

4.3. Future Work

All of the information gathered to this point and that will be gathered in projects such as these is important for the evolution of QD devices for light harvesting and emitting applications. It is vital to be able to understand and tune the charge transfer into or out of a QD in order for them to prove useful in devices. Clearly there are still misunderstandings prevalent regarding the phenomena that occur within QDs and of charge carrier dynamics in QD-ligand systems.

Future work on this project should include experiments that probe temperature dependence. A model that can describe a system at all temperatures is much more thorough. Temperature dependent studies are also capable of pointing out further modeling flaws and would allow for them to be tweaked and hopefully perfected. Specifically, the current issue of our fitting model not being able to differentiate enthalpy and number of QD binding sites would be solved through these experiments.

It has become apparent that the independent binding site model is rather complicated, especially when trying to create a model that will take into account desorption heats of a native ligand and adsorption heats of another ligand type. However, once these interactions are accounted for, it is a distinct possibility that this model will lead to a vast knowledge of QD-ligand systems while also yielding greater accuracy than a Langmuir analysis, even for quenching ligands.

In future, other ligands and their interaction with QDs should be explored. In direct response to this study, data obtained from Ph_2Bts^{Me} should be done to complete the comparison of this series of R_2Bts^{Me} ligands. From the data obtained so far, the thioether group itself may not be a strong enough nucleophile when taking into account the low

site association constants. Reproducibility of useful data from the ITC becomes difficult when ligands do not bind strongly to sample QDs. Since most QDs are stabilized in organic solvent by TOPO, which has been experimentally shown to have a site association constant of approximately 33 M^{-1}, ligands with association constants greater than this value would be likely to participate in ligand exchange interactions. This would eliminate having to completely wash TOPO off of the QD surfaces and risk damage to the QDs. Eliminating this step would also make passivation of the QDs using the experimental ligand also not necessary. Compounds that bind more strongly to the surface of QDs would lead to greater site association constants and more validity with ITC data. This will help make PL and ITC experiments easier, quicker, and more reproducible. The stronger binding may properly prove that ITC can be a useful method when determining association and charge transfer values, and can be implemented regardless of a ligand's effect on PL.

REFERENCES

(1) Zhang, J. Z. *Optical Properties and Spectroscopy of Nanomaterials*; World Scientific: New Jersey, **2009**.

(2) Bawendi, M. G.; Steigerwald, M. L.; Brus, L. E. *Annu. Rev. Phys.* **1990**, *41*, 477.

(3) Moule, A. J.; Chang, L. L.; Thambidurai, C.; Vidu, R.; Stroeve, P. *J. Mater. Chem.* **2012**, *22*, 2351.

(4) Ahmadi, M.; Pramana, S. S.; Xi, L. F.; Boothroyd, C.; Lam, Y. M.; Mhaisalkar, S. *J. Phys. Chem. C* **2012**, *116*, 8202.

(5) Salant, A.; Shalom, M.; Tachan, Z.; Buhbut, S.; Zaban, A.; Banin, U. *Nano Letters* **2012**, *12*, 2095.

(6) Yaacobi-Gross, N.; Soreni-Harari, M.; Zimin, M.; Kababya, S.; Schmidt, A.; Tessler, N. *Nat. Mater.* **2011**, *10*, 974.

(7) McDaniel, H.; Fuke, N.; Pietryga, J. M.; Klimov, V. I. *Journal of Physical Chemistry Letters* **2013**, *4*, 355.

(8) Albero, J.; Martinez-Ferrero, E.; Ajuria, J.; Waldauf, C.; Pacios, R.; Palomares, E. *Physical Chemistry Chemical Physics* **2009**, *11*, 9644.

(9) Nadarajah, A.; Smith, T.; Konenkamp, R. *Nanotechnology* **2012**, 23.

(10) Noone, K. M.; Subramaniyan, S.; Zhang, Q. F.; Cao, G. Z.; Jenekhe, S. A.; Ginger, D. S. *J. Phys. Chem. C* **2011**, *115*, 24403.

(11) Dias, E. A.; Saari, J. I.; Tyagi, P.; Kambhampati, P. *J. Phys. Chem. C* **2012**, *116,* 5407.

(12) Signorini, R.; Fortunati, I.; Todescato, F.; Gardin, S.; Bozio, R.; Jasieniak, J. J.; Martucci, A.; Della Giustina, G.; Brusatin, G.; Guglielmi, M. *Nanoscale* **2011**, *3*, 4109.

(13) Zavelani-Rossi, M.; Lupo, M. G.; Krahne, R.; Manna, L.; Lanzani, G. *Nanoscale* **2010**, *2*, 931.

(14) Thoma, J.; Liang, B. L.; Lewis, L.; Hegarty, S. P.; Huyet, G.; Huffaker, D. L. *Applied Physics Letters* **2013**, *102*.

(15) Zhao, L. J.; Hu, L. F.; Fang, X. S. *Adv. Funct. Mat.* **2012**, *22*, 1551.

(16) Haffouz, S.; Barrios, P. J.; Normandin, R.; Poitras, D.; Lu, Z. *Opt. Lett.* **2012**, *37*, 1103.

(17) Yuan, Y.; Riehle, F. S.; Nitschke, R.; Kruger, M. *Mater. Sci. Eng. B-Adv. Funct. Solid-State Mater.* **2012**, *177*, 245.

(18) Shirasaki, Y.; Supran, G. J.; Bawendi, M. G.; Bulovic, V. *Nat. Photonics* **2013**, *7*, 13.

(19) Michalet, X.; Pinaud, F.; Lacoste, T. D.; Dahan, M.; Bruchez, M. P.; Alivisatos, A. P.; Weiss, S. *Single Molecules* **2001**, *2*, 261.

(20) Petryayeva, E.; Krull, U. J. *Langmuir* **2012**, *28*, 13943.

(21) Norris, D. J.; Efros, A. L.; Rosen, M.; Bawendi, M. G. *Phys. Rev. B* **1996**, *53*, 16347.

(22) Protasenko, V.; Bacinello, D.; Kuno, M. *J. Phys. Chem. B* **2006**, *110*, 25322.

(23) Kopping, J. T.; Patten, T. E. *J. Am. Chem. Soc.* **2008**, *130*, 5689.

(24) Min, W. J.; Jung, S.; Lim, S. J.; Kim, Y.; Shin, S. K. *J. Phys. Chem. A* **2009**, *113*, 9588.

(25) Clapp, A. R.; Goldman, E. R.; Mattoussi, H. *Nature Protocols* **2006**, *1*, 1258.

(26) Foos, E. E.; Wilkinson, J.; Makinen, A. J.; Watkins, N. J.; Kafafi, Z. H.; Long, J. P. *Chem. Mat.* **2006**, *18*, 2886.

(27) Morris-Cohen, A. J.; Vasilenko, V.; Amin, V. A.; Reuter, M. G.; Weiss, E. A. *ACS Nano* **2012**, *6*, 557.

(28) Munro, A. M.; Jen-La Plante, I.; Ng, M. S.; Ginger, D. S. *J. Phys. Chem. C* **2007**, *111*, 6220.

(29) Korala, L.; Brock, S. L. *J. Phys. Chem. C* **2012**, *116*, 17110.

(30) Green, M. *J. Mater. Chem.* **2010**, *20*, 5797.

(31) Guyot-Sionnest, P.; Wehrenberg, B.; Yu, D. *J. Chem. Phys.* **2005**, *123*.

(32) Pradhan, N.; Reifsnyder, D.; Xie, R. G.; Aldana, J.; Peng, X. G. *J. Am. Chem. Soc.* **2007**, *129*, 9500.

(33) Puzder, A.; Williamson, A. J.; Zaitseva, N.; Galli, G.; Manna. L.; Alivisatos, A. P. *Nano Letters* **2004**, *4*, 2361.

(34) Smith, A. M.; Duan, H. W.; Rhyner, M. N.; Ruan, G.; Nie, S. M. *Phys. Chem. Chemical Physics* **2006**, *8*, 3895.

(35) Wang, W.; Banerjee, S.; Jia, S. G.; Steigerwald, M. L.; Herman, I. P. *Chem. Mat.* **2007**, *19*, 2573.

(36) Yin, Y.; Alivisatos, A. P. *Nature* **2005**, *437*, 664.

(37) Ning, Z. J.; Molnar, M.; Chen, Y.; Friberg, P.; Gan, L. M.; Agren, H.; Fu, Y. *Phys. Chem. Chemical Physics* **2011**, *13*, 5848.

(38) Knowles, K. E.; Tice, D. B.; McArthur, E. A.; Solomon, G. C.; Weiss, E. A. *J. Am. Chem. Soc.* **2010**, *132*, 1041.

(39) Williams, E. S.; Major, K. J.; Tobias, A.; Woodall, D.; Morales, V.; Lippincott, C.; Moyer, P. J.; Jones, M. *J. Phys. Chem. C* **2013**, *117*, 4227.

(40) Boldt, K.; Jander, S.; Hoppe, K.; Weller, H. *ACS Nano* **2011**, *5*, 8115.

(41) Dorokhin, D.; Tomczak, N.; Velders, A. H.; Reinhoudt, D. N.; Vancso, G. J. *J. Phys. Chem. C* **2009**, *113*, 18676.

(42) Greenham, N. C.; Peng, X. G.; Alivisatos, A. P. *Phys. Rev. B* **1996**, *54*, 17628.

(43) Koole, R.; Schapotschnikow, P.; Donega, C. D.; Vlugt, T. J. H.; Meijerink, A. *ACS Nano* **2008**, *2*, 1703.

(44) Landes, C. F.; Braun, M.; El-Sayed, M. A. *J. Phys. Chem. B* **2001**, *105*, 10554.

(45) Morris-Cohen, A. J.; Frederick, M. T.; Cass, L. C.; Weiss, E. A. *Abstr. Pap. Am. Chem. Soc.* **2011**, *242*.

(46) Szendrei, K.; Jarzab, D.; Yarema, M.; Sytnyk, M.; Pichler, S.; Hummelen, J. C.; Heiss, W.; Loi, M. A. *J. Mater. Chem.* **2010**, *20*, 8470.

(47) Chen, H. Y.; Lo, M. K. F.; Yang, G. W.; Monbouquette, H. G.; Yang, Y. *Nat. Nanotechnol.* **2008**, *3*, 543.

(48) Xu, S. H.; Wang, C. L.; Cui, Y. P. *Theochem-J. Mol. Struct.* **2009**, *916*, 168.

(49) Bullen, C.; Mulvaney, P.; *Langmuir* **2006**, *22*, 3007.

(50) Albero, J.; Martinez-Ferrerro, E.; Iacopino, D.; Vidal-Ferran, A.; Palomares, E. *Physical Chemistry Chemical Physics* **2010**, *12*, 13047.

(51) Tan, Y. Z.; Jin, S.; Hamers, R. J. *J. Phys. Chem. C* **2013**, *117*, 313.

(52) Donakowski, M. D.; Godbe, J. M.; Sknepnek, R.; Knowles, K. E.; de la Cruz, M. O.; Weiss, E. A. *J. Phys. Chem. C* **2010**, *114*, 22526.

(53) Landes, C.; El-Sayed, M. A. *J. Phys. Chem. A* **2002**, *106*, 7621.

(54) Sharma, S. N.; Pillai, Z. S.; Kamat, P. V. *J. Phys. Chem. B* **2003**, *107*, 10088.

(55) Stern, O.; Volmer, M. *Physikalische Zeitschrift* **1919**, *20*, 183.

(56) Yu, W. W.; Qu, L. H.; Guo, W. Z.; Peng, X. G.; *Chem. Mat.* **2003**, *15*, 2854.

(57) Baker, D. R.; Kamat, P. V. *Langmuir* **2010**, *26*, 11272.

(58) Liu, I. S.; Lo, H. H.; Chien, C. T.; Lin, Y. Y.; Chen, C. W.; Chen, Y. F.; Su, W. F.; Liou, S. C. *J. Mater. Chem.* **2008**, *18*, 675.

(59) Uematsu, T.; Waki, T.; Torimoto, T.; Kuwabata, S. *J. Phys. Chem. C* **2009**, *113*, 21621.

(60) Koposov, A. Y.; Szymanski, P.; Cardolaccia, T.; Meyer, T. J.; Klimov, V. I.; Sykora, M. *Adv. Funct. Mater.* **2011**, *21*, 3159.

(61) Williams, E. S. M.S. Dissertation, The University of North Carolina at Charlotte, 2013.

(62) Marcus, R. A. *J. Phys. Chem.* **1989**, *93*, 3078.

(63) Closs, G. L.; Calcaterra, L. T.; Green, N. J.; Penfield, K. W.; Miller, J. R. *J. Phys. Chem.* **1986**, *90*, 3673.

(64) Freire, E.; Mayorga, O. L.; Straume, M. *Anal. Chem.* **1990**, *62*, A950.

(65) Cedervall, T.; Lynch, I.; Lindman, S.; Berggard, T.; Thulin, E.; Nilsson, H.; Dawson, K. A.; Linse, S. *Proc. Natl. Acad. Sci. U. S. A.* **2007**, *104*, 2050.

(66) Wang, X.; Matei, E.; Gronenborn, A. M.; Ramstrom, O.; Yan, M. D. *Anal. Chem.* **2012**, *84*, 4248.

(67) Alston, J. R.; Overson, D.; Poler, J. C.; *Langmuir* **2012**, *28*, 264.

(68) Grote, C.; Chiad, K. J.; Vollmer, D.; Garnweitner, G. *Chem. Commun.* **2012**, *48*, 1464.

(69) Shen, Y.; Tan, R.; Gee, M. Y.; Greytak, A. B. *ACS Nano* **2015**, *9* (3), 3345.

(70) Demarse, N. A.; Quinn, C. F.; Eggett, D. L.; Russell, D. J.; Hansen, L. D. *Analytical Biochemistry* **2011**, *417*, 247.

(71) Lozano-Lewis, L. I.; John-Rajkumar, S. V.; Islas, S. A.; Pike, R. D.; Rabinovich, D. *Main Group Chem.* **2007**, *6*, 133.

(72) Lozano-Lewis, L. I. M.S. Dissertation, The University of North Carolina at Charlotte, 2006.

(72) Morris-Cohen, A. J.; Frederick, M. T.; Lilly, G. D.; McArthur, E. A.; Weiss, E. A. *Journal of Physical Chemistry Letters* **2010**, *1*, 1078.

(73) Wang, F.; Tang, R.; Kao, J. L. F.; Dingman, S. D.; Buhro, W. E. *J. Am. Chem. Soc.* **2009**, *131*, 4983.

(74) Fischer, S. A.; Crotty, A. M.; Kilina, S. V.; Ivanov, S. A.; Tretiak, S. *Nanoscale* **2012**, *4*, 904.

(75) Kilina, S.; Ivanov, S.; Tretiak, S. *J. Am. Chem. Soc.* **2009**, *131*, 7717.

(76) Al-Salim, N.; Young, A. G.; Tilley, R. D.; McQuillan, A. J.; Xia, J. *Chem. Mat.* **2007**, *19*, 5185.

(77) Eilon, M. J.; Mokari, T.; Banin, U. *J. Phys. Chem. B* **2001**, *105*, 12726.

(78) Katari, J. E. B.; Colvin, V. L.; Alivisatos, A. P. *J. Phys. Chem.* **1994**, *98*, 4109.

(79) Young, A. G.; Al-Salim, N.; Green, D. P.; McQuillan, A. J. *Langmuir* **2008**, *24*, 3841.

(80) Lorenz, J. K.; Ellis, A. B. *J. Am. Chem. Soc.* **1998**, *120*, 10970.

(81) Bussian, D. A.; Malko, A. V.; Htoon, H.; Chen, Y. F.; Hollingsworth, J. A.; Klimov, V. I. *J. Phys. Chem. C* **2009**, *113*, 2241.

(82) Califano, M.; Franceschetti, A.; Zunger, A. *Phys. Rev. B* **2007**, *75*.

(83) Crooker, S. A.; Barrick, T.; Hollingsworth, J. A.; Klimov, V. I. *Applied Physics Letters* **2003**, *82*, 2793.

(84) Donega, C. D.; Bode, M.; Meijerink, A. *Phys. Rev. B* **2006**, *74*.

(85) Labeau, O.; Tamarat, P.; Lounis, B. *Phys. Rev. Letters* **2003**, *90*.

(86) Califano, M.; Franceschetti, A.; Zunger, A. *Nano Letters* **2005**, *5*, 2360.

(87) McArthur, E. A.; Morris-Cohen, A. J.; Knowles, K. E.; Weiss, E. A. *J. Phys. Chem. B* **2010**, *114*, 14514.

(88) Xiao, Q.; Xiao, C. *Applied Surface Science* **2009**, *255*, 7111.

(89) Jones, M.; Lo, S. S.; Scholes, G. D. *J. Phys. Chem. C* **2009**, *113*, 18632.

(90) Jones, M.; Lo, S. S.; Scholes, G. D. *Proc. Natl. Acad. Sci. U. S. A.* **2009**, *106*, 3011.

(91) Guyot-Sionnest, P.; Shim, M.; Matranga, C.; Hines, M. *Phys. Rev. B* **1999**, *60*, R2181.

(92) Gooding, A. K.; Gomez, D. E.; Mulvaney, P. *ACS Nano* **2008**, *2*, 669.

(93) Hess, B. C.; Okhrimenko, I. G.; Davis, R. C.; Stevens, B. C.; Schulzke, Q. A.; Wright, K. C.; Bass, C. D.; Evans, C. D.; Summers, S. L. *Phys. Rev. Letters* **2001**, *86*, 3132.

(94) Burda, C.; Link, S.; Mohamed, M.; El-Sayed, M. *J. Phys. Chem. B* **2001**, *105*, 12286.

(95) Burda, C.; Link, S.; Mohamed, M. B.; El-Sayed, M. *J. Chem. Phys.* **2002**, *116*, 3828.

(96) Klimov, V. I.; Mikhailovsky, A. A.; McBranch, D. W.; Leatherdale, C. A.; Bawendi, M. G. *Phys. Rev. B* **2000**, *61*, 13349.

(97) Knowles, K. E.; McArthur, E. A.; Weiss, E. A. *ACS Nano* **2011**, *5*, 2026.

(98) Jones, M.; Scholes, G. D.; *J. Mater. Chem.* **2010**, *20*, 3533.

(99) Tobias, A. M.S. Dissertation, The University of North Carolina at Charlotte, 2012.

(100) Wilcox, D. E. *Inorganica Chimica Acta* **2008**, *361*, 857.

(101) Wang, Y. *Acc. Chem. Res.* **1991**, *24*, 133.

(102) Grossoehme, N. E.; Spuches, A. M.; Wilcox, D. E. *J. Biol. Inorg. Chem.* **2010**, *15*, 1183.

(103) Emerson, J. P.; Le, V. H.; Lewis, E. A. *eLS. John Wiley & Sons, Ltd: Chichester* **2012**, 1. DOI: 10.1002/9780470015902.a0003010.pub3

(104) Brown, W. H. *Introduction to Organic Chemistry,* 2nd Ed.; Saunders College Publishing: **2000**.